April 1999 • NREL/SR-520-26315

Subcontractor Report

# Device Physics of Thin-Film Polycrystalline Cells and Modules

## December 6, 1993 – March 31, 1998

James R. Sites
*Department of Physics*
*Colorado State University*
*Ft. Collins, Colorado*

NREL
National Renewable Energy Laboratory
1617 Cole Boulevard
Golden, Colorado 80401-3393

NREL is a U.S. Department of Energy Laboratory
Operated by Midwest Research Institute • Battelle • Bechtel

Contract No. DE-AC36-98-GO10337

April 1999 • NREL/SR-520-26315

# Device Physics of Thin-Film Polycrystalline Cells and Modules

## December 6, 1993 – March 31, 1998

James R. Sites
*Department of Physics*
*Colorado State University*
*Ft. Collins, Colorado*

NREL Technical Monitor: B. von Roedern

Prepared under Subcontract No. XAX-4-14000-01

National Renewable Energy Laboratory

1617 Cole Boulevard
Golden, Colorado 80401-3393

NREL is a U.S. Department of Energy Laboratory
Operated by Midwest Research Institute • Battelle • Bechtel

Contract No. DE-AC36-98-GO10337

**NOTICE**

This report was prepared as an account of work sponsored by an agency of the United States government. Neither the United States government nor any agency thereof, nor any of their employees, makes any warranty, express or implied, or assumes any legal liability or responsibility for the accuracy, completeness, or usefulness of any information, apparatus, product, or process disclosed, or represents that its use would not infringe privately owned rights. Reference herein to any specific commercial product, process, or service by trade name, trademark, manufacturer, or otherwise does not necessarily constitute or imply its endorsement, recommendation, or favoring by the United States government or any agency thereof. The views and opinions of authors expressed herein do not necessarily state or reflect those of the United States government or any agency thereof.

Available to DOE and DOE contractors from:
Office of Scientific and Technical Information (OSTI)
P.O. Box 62
Oak Ridge, TN 37831
Prices available by calling 423-576-8401

Available to the public from:
National Technical Information Service (NTIS)
U.S. Department of Commerce
5285 Port Royal Road
Springfield, VA 22161
703-605-6000 or 800-553-6847
or
DOE Information Bridge
http://www.doe.gov/bridge/home.html

Printed on paper containing at least 50% wastepaper, including 20% postconsumer waste

# SUMMARY

The results of the subcontract effort included progress in understanding CdTe and $Cu(In_{1-x}Ga_x)Se_2$ based solar cells, in developing additional measurement and analysis techniques at the module level, and in strengthening collaboration within the thin-film polycrystalline solar-cell community.

A major part of the CdTe work consisted of elevated-temperature stress tests to determine fabrication and operation conditions that minimize the possibility of long-term performance changes. Other CdTe studies included analysis of the back-contact junction, complete photon accounting, and the tradeoff with thin CdS between photocurrent gain and voltage loss.

The $Cu(In_{1-x}Ga_x)Se_2$ studies included work on the role of sodium in enhancing performance, the conditions under which conduction-band offsets affect cell performance, the transient effects of cycling between light and dark conditions, and detailed analysis of several individual series of cells.

One aspect of thin-film module analysis has been addressing the differences in approach needed for relatively large individual cells made without grids. Most work, however, focused on analysis of laser scanning data, including defect signatures, photocurrent/shunting separation, and the effects of forward bias or high-intensity light.

Collaborations with other labs continued on an individual basis, and starting in 1994, through the national R & D photovoltaic teams. Colorado State has been heavily involved in the structure and logistics of both the CdTe and CIS teams, as well as making, frequent technical contributions in both areas.

## TABLE OF CONTENTS

SUMMARY ..... i

FIGURES ..... iii

INTRODUCTION ..... 1

CdTe CELL ANALYSIS ..... 2

- Temperature Stress Tests ..... 2
- Back Barrier ..... 7
- Photon Losses ..... 9
- CdS Thickness ..... 12

CIS/CIGS CELL ANALYSIS ..... 17

- Sodium Effects ..... 17
- Band-Offset Effects ..... 19
- Temperature Stress ..... 24
- Other CIS Measurements ..... 26

MODULE ANALYSIS ..... 32

- Cell Geometry ..... 32
- Laser Scanning ..... 35
- Defect Signatures ..... 35
- Photocurrent/S hunting Separation ..... 37
- Forward Bias/High Intensity ..... 39

STATUS OF THIN-FILM POLYCRYSTALLINE CELLS ..... 42

COMMUNICATIONS ..... 48

- Publications ..... 48
- Graduate Degrees ..... 50
- Presentations ..... 50

# FIGURES


Figure 1. CdTe J-V curves following high-temperature stress ..... 3
Figure 2. Effect of stress on individual parameters ..... 4
Figure 3. Biases used in stress tests ..... 6
Figure 4. Efficiency change at different biases ..... 6
Figure 5. CdTe back-contract model ..... 7
Figure 6. Back-contact J-V temperature effect ..... 8
Figure 7. Back-contact effect on fill-factor and efficiency ..... 8
Figure 8. CdTe quantum efficiency and photon losses ..... 10
Figure 9. Transmission and reflection of CdTe cell layers ..... 11
Figure 10. QE for different CdS thicknesses ..... 13
Figure 11. CdTe photocurrent variation with CdS Thickness ..... 14
Figure 12. Voltage and fill-factor vs. CdS absorption ..... 14
Figure 13. Comparison of high-efficiency CdTe cells ..... 16
Figure 14. Variation of CIS voltage and fill-factor with sodium ..... 18
Figure 15. Calculated CIS efficiency dependence on band offset ..... 20
Figure 16. Contrast of n and $n^-$ CdS on CIS JV curves ..... 22
Figure 17. Explanation of n vs. $n^-$ effect ..... 23
Figure 18. CIS JV curves before and after temperature stress ..... 25
Figure 19. CIS Capacitance before and after temperature stress ..... 27
Figure 20. Effect of high-resistivity ZnO thickness ..... 28
Figure 21. Current-voltage for electrodeposited CIGS ..... 29
Figure 22. Comparison of highest-efficiency NREL CIGS cells ..... 31
Figure 23. Module cell geometry with current flow ..... 32

Figure 24. JV contrast of research and module cells ..... 33
Figure 25. Distributed vs. linear series resistance ..... 34
Figure 26. Large-scale laser scanner at NREL ..... 35
Figure 27. Calculated laser scan with shunt present ..... 36
Figure 28. Shunt vs. photocurrent-defect signatures ..... 37
Figure 29. CIGS line scans at different frequencies ..... 38
Figure 30. Short-circuit vs. forward-bias line seams ..... 39
Figure 31. Laser-scan signal vs. series resistance ..... 40
Figure 32. CdTe line scans vs. voltage and intensity ..... 40
Figure 33. Highest-efficiency JV curves ..... 43
Figures 34. Losses in highest-efficiency cells ..... 47

## TABLES

Table 1. Percentage changes in CdTe efficiency ..... 6
Table 2. Parameters for highest-efficiency cells ..... 44
Table 3. Loss comparison in highest-efficiency cells ..... 44

# INTRODUCTION

The objectives of the Colorado State University (CSU) program have been (1) the separation and quantification of individual losses in specific thin-film solar cells, (2) the detailed characterization of small modules, and (3) the presentation of a viable model for the forward-current loss mechanism.

Most of the experimental and analytical work has been done by a group of dedicated research students: Xiaoxiang Liu completed her Ph.D. in 1994 and now teaches at Brookdale Community College in New Jersey. Ingrid Eisgruber finished her doctoral degree the following year and is very active in solar-cell research at the Materials Research Group in Golden, Colorado. Jennifer Granata is in the final stages of her Ph.D. program, and Jason Hiltner has recently passed his Ph.D. candidacy Exam. Gunther Stollwerck wrote his M.S. thesis in 1995 and is in the final part of his Ph.D. work in Freiberg, Germany. In addition, Jon Sharp, Karl Schmidt, and Brendon Murphy, at the Master's level, and Harry Sax at the undergraduate level, contributed important project-level studies to the work reported her.

The Colorado State group has been an active part of the NREL-sponsored National CdTe and CIS R & D Teams. It has had active collaborations with researchers at the Colorado School of Mines, Energy Photovoltaics, Inc., Golden Photon, Inc., the Institute of Energy Conversion, International Solar Electric Technology, Inc., the National Renewable Energy Laboratory, Siemens Solar Industries, Solar Cells, Inc., Solarex, the University of South Florida, and the University of Toledo.

# CdTe CELL ANALYSIS

## Temperature Stress Tests

A significant addition to the Colorado State experimental facilities has been the construction of apparatus for temperature stress measurements. It consists of an oven for dark stress tests and three independently illuminated areas for light stress tests. Each area can accommodate a substrate with multiple cells or a small module. Individual cells can be attached to various load resistors or external biases. To date temperature-stress tests have been done primarily with CdTe cells.

CdTe modules, especially those made by Solar Cells, Inc. (SCI), have shown very good outdoor stability for 2-3 year testing periods. On the other hand, changes in CdTe cell performance, particularly following prolonged temperatures in the 100° C range, have been noticed by various labs. Our goal as part of the National CdTe R & D Team has been to systematically stress, measure, and analyze such cells.

Fig. 1 shows room-temperature current-voltage characteristics for a reasonably typical SCI cells following various periods of time at or slightly above 100° C. These cells initially had $J_{sc}$ ~ 20 mA/cm$^2$, $V_{oc}$ ~ 820 mV, ff ~ 0.7, and efficiencies of 11-12%. The top shows a cell held under illumination of nearly two suns, and bottom shows a nominally identical cell held in the dark at a similar temperature. Clearly the changes occur more rapidly under illumination. In these initial measurements, however, the cells were not contacted during stress, so the dark bias was zero, and the light bias was $V_{oc}$, or about 700 mV at the elevated temperature.

Fig. 2 shows the evolution of open-circuit voltage, fill-factor, and short-circuit current measured at room temperature following the high-temperature stresses. When the stresses were repeated on other SCI cells, the results were always similar to those shown. The following features were seen:

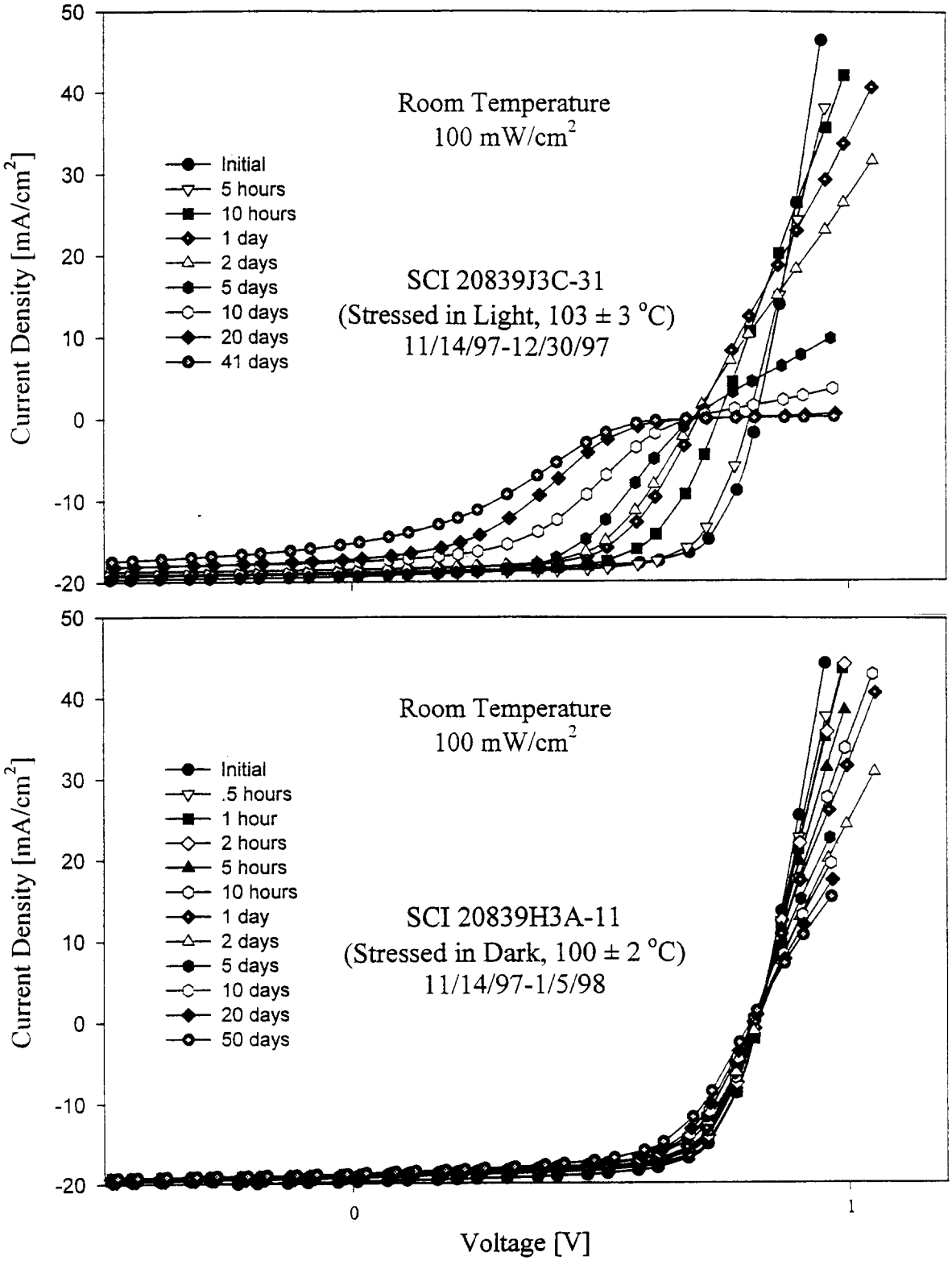


**Fig. 1. CdTe current-voltage curves following high-temperature stress in light and dark.**

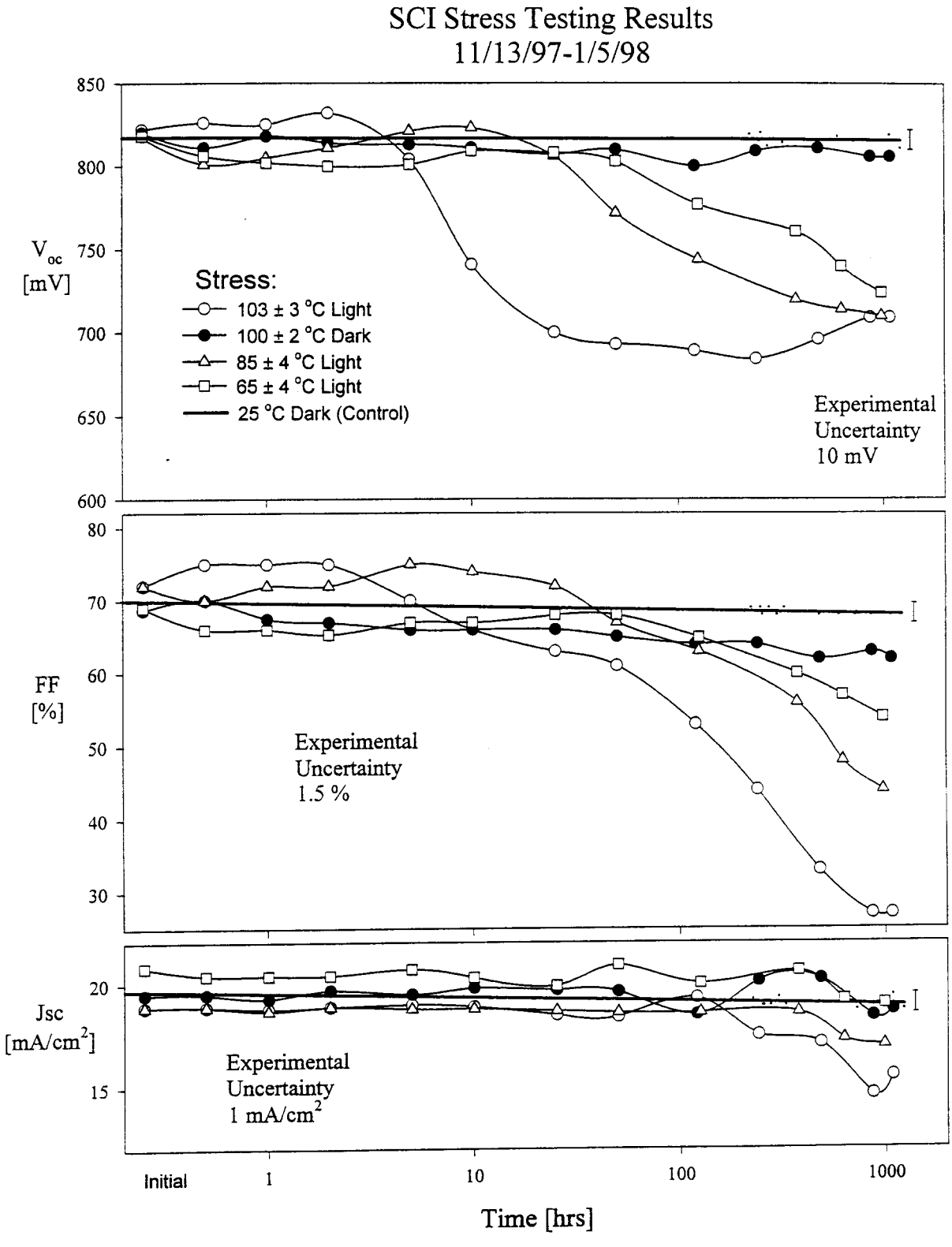


**Fig. 2. Effect of temperature stress on individual parameters.**

(1) An initial small increase in fill-factor, interpreted as an improved back contact or less "rollover."

(2) At a slightly later time, the onset of a drop in $V_{oc}$, which would eventually be as much as 20%.

(3) At a still later time, a drop in fill-factor which could eventually be more than a factor of two.

(4) At still later times, an extreme forward-current, or "rollover," limitation.

(5) Little or no change in $J_{sc}$, or quantum efficiency (QE) curves, until the dominance of the forward-current limitation. Then a larger QE drop at the shorter wavelengths.

(6) A significant drop in carrier density within the CdTe absorber deduced from capacitance measurements.

(7) A slower pattern of changes at lower temperatures (~ 20 times slower at 65° C. under illumination that at 100° C.) Activation energies of 1 - 1.5 eV are implied.

(8) Changes much slower in the dark than in the light.

(9) There are likely two mechanisms involved, one changing the back-contact barrier and one degrading the primary junction. A possible explanation is movement of a species such as copper, which could be responsible for changes at both the front and the back of the cell.

Additional measurements on similar SCI cells have at least partially resolved whether light or bias drives the high-temperature changes seen. Fig. 3 shows how seven different bias conditions were defined. R is the maximum-power load resistance, which is slightly less at elevated temperatures. R/2 defines a point on the curve intermediate between short-circuit and R, and 2R is intermediate between R and open-circuit. The $V < 0$ bias is chosen to be approximately equal in magnitude to $V_{MP}$, and $J > 0$ corresponds to a current of the same magnitude as $J_{MP}$. Fig. 4, taken from two columns of Table I, clearly shows a plateau of small efficiency decrease between short-circuit and maximum-power. In reverse bias, or at open-circuit and above, the changes are significantly more rapid. At short times, the increased efficiencies correspond to the initial improvement in the back contact barrier discussed above and in the following section.

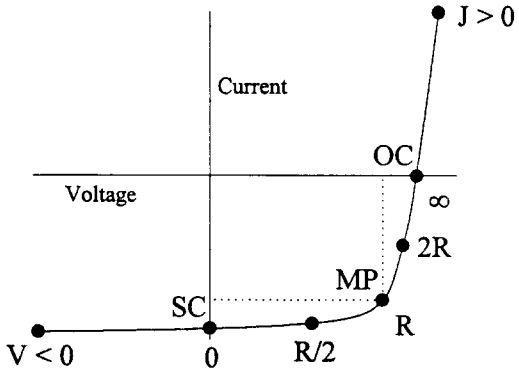


**Fig. 3. Bias conditions used in stress tests.**

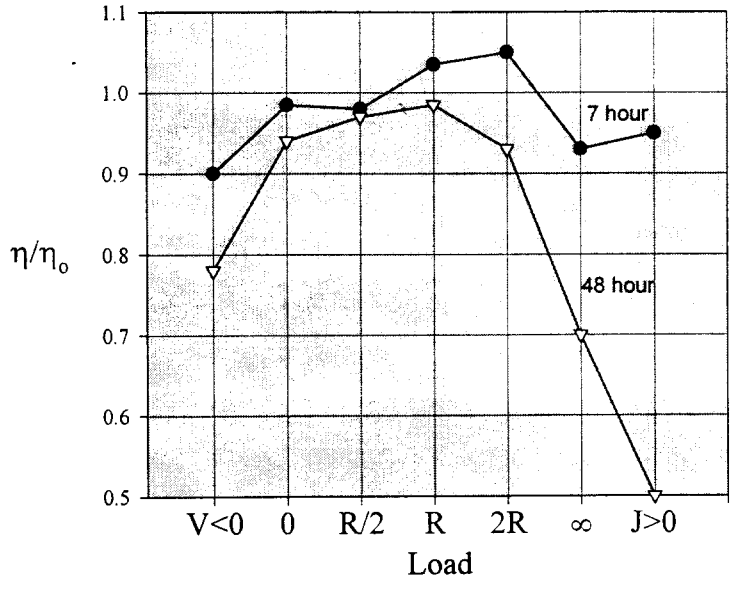


**Fig. 4. Changes with temperature-stress at different biases.**

| Load | 2 hr | 7 hr | 24 hr | 48 hr |
|---|---|---|---|---|
| V<0 | -7.5 | -10 | -16 | -22 |
| 0 | -1 | -1.5 | -3.5 | -6 |
| R/2 | -2 | -2 | -2 | -3 |
| R | +3 | +3.5 | +3.5 | -1.5 |
| 2R | +7 | +5 | -1 | -7 |
| ∞ | +4 | -7 | -26 | -30 |
| J>0 | +3.5 | -5 | -22 | -50 |

**Table I. Percentage changes in efficiency (average of two cells).**

## BACK BARRIER

A reasonable model for the CdTe back contact is shown in Fig. 5 (see Publ. 10). The band diagram indicates a 4 μm CdTe layer which is nearly depleted throughout. The curvature near the back contact indicates a diode of opposite polarity to the primary junction. The magnitude of the back-barrier must be less than that of the primary junction. The 0.3 eV indicated is typical of many CdTe contacts. (Some authors define the barrier with respect to the Fermi level, which gives numerically large values.)

The band structure and circuit diagram in Fig. 5 leads to calculated J-V curves very similar to the experimental data shown in Fig. 6 from an ANTEC CdTe cell. In general, the back-contact diode must be assumed to be somewhat leaky to fit the data. Such leakage is very plausible for a low-barrier diode on a non-homogenous surface. Data comparable to Fig. 6 for other CdTe cells will have larger or smaller amounts of current-limitation, commonly referred to as "rollover." The onset of rollover for CdTe cells is typically slightly above or slightly below room temperature and can usually be modeled with a single barrier-height parameter.

The impact of a back barrier on cell performance can be very modest even when the rollover appears significant, as for example with the low temperature curves in Fig. 6. The impact of barrier height on room-temperature fill-factor, and hence efficiency, is illustrated in Fig. 7. 300 meV is a reasonable delineation between "significant' and "insignificant" barriers. However, rollover, such as shown in Fig. 6, can be an important precursor of possible trouble. If, for example, a new cell has a barrier just below 300 meV, but it increases as the cell ages, one may at later times see performance degradation similar to that discussed in the previous section on stress tests.

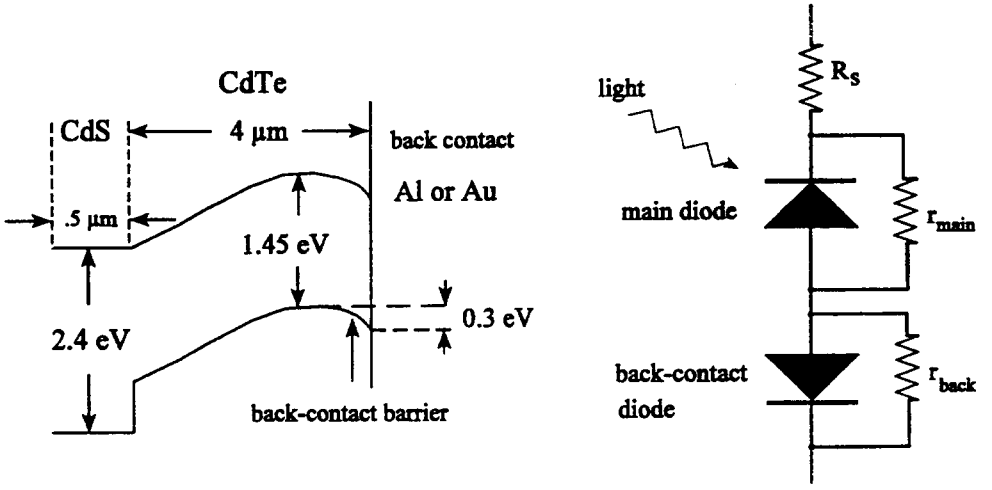


**Fig. 5. Band structure and circuit model illustrating CdTe back contact barrier.**

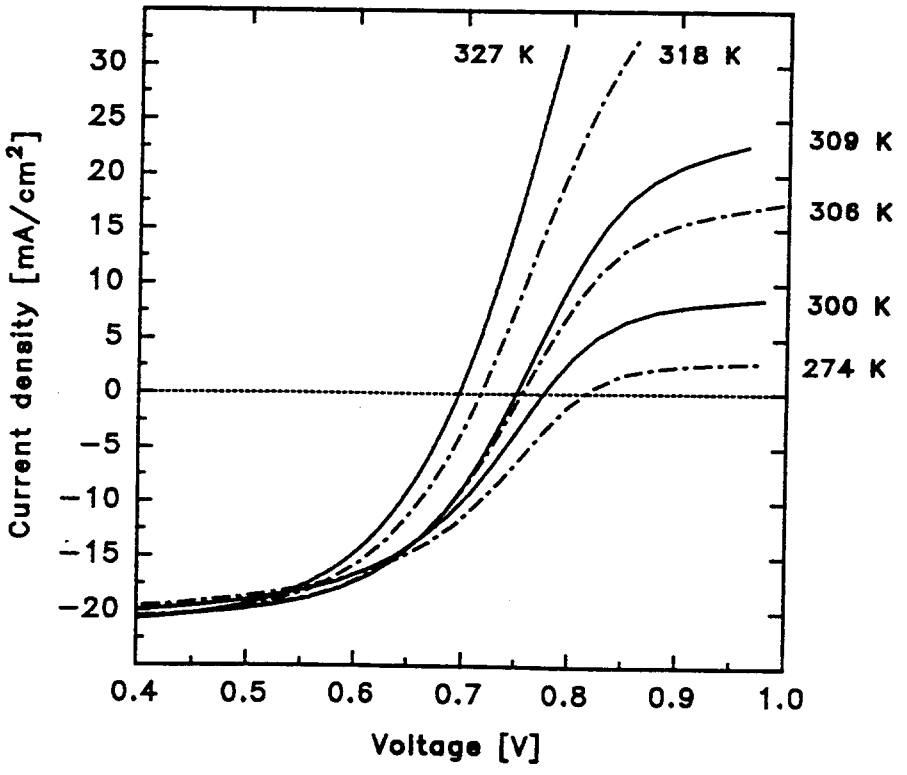


**Fig. 6. Temperature dependence of back-contact barrier effect (ANTEC CdTe cell).**

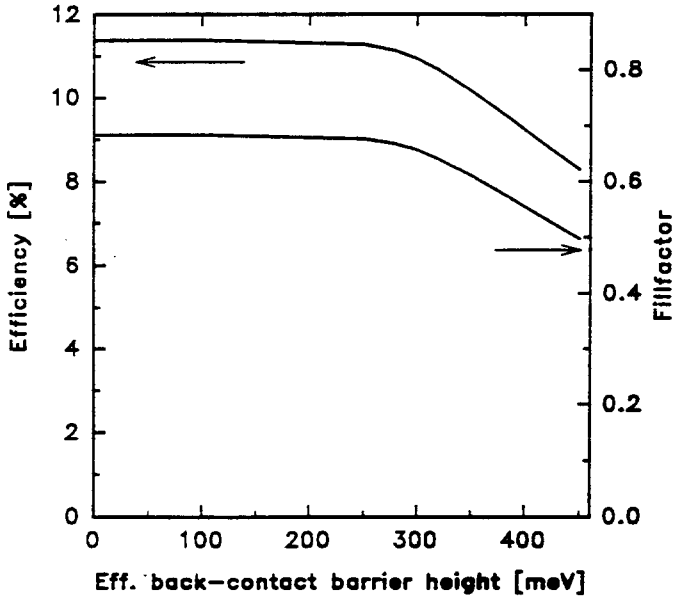


**Fig. 7. Variation in fill-factor and efficiency with height of back-barrier**

**Photon Losses**

The quantum efficiency (QE) of a solar cell yields a great deal of information about the cell's photon losses. Fig. 8 shows the measured QE of a CdTe cell. It clearly shows the short-wavelength cut-off due to the CdS window used and the long-wavelength cut-off that corresponds well to the expected CdTe bandgap. The integrated QE, multiplied by the solar spectrum, expressed in appropriate units, yields the photocurrent for that spectrum. Integration of unity QE up to the absorber bandgap, and zero beyond, gives the maximum photocurrent for the spectrum used.

Between the measured QE and unity lie various photon losses. For most cells these losses can be quantitively separated if the necessary optical measurements can be made. Fig. 9 shows the measured transmission (top) and reflection (bottom) after each layer of cell fabrication: glass superstrate only, glass plus $SnO^2$ contact, glass plus $SnO_2$ plus CdS window, and completed cell. The middle part of Fig. 9 shows the absorption of each layer deduced from the transmission and reflection data. This information is then used to divide the photon-loss region of Fig. 8 appropriately and, for example, to separate the less-than-unity collection efficiency of deeply penetrating red photons from optical absorption.

The integration of each loss region in Fig. 8, again weighted by the assumed spectrum gives the quantitative reduction of photocurrent for that mechanism. Mathematically, these losses are constrained to add to the difference between actual and maximum photocurrent. In some cases, the clearly deduced optical losses deduced as shown in Fig. 9 do not account for the full reduction in QE. In this case, we typically add, and quantify, an "unknown" photon loss. The quantified losses shown at the bottom of Fig. 8 have a strong utilitarian value in that they cleanly identify large vs. small losses and tell the cell fabricator how much potential improvement exists in possible changes to the cell components.

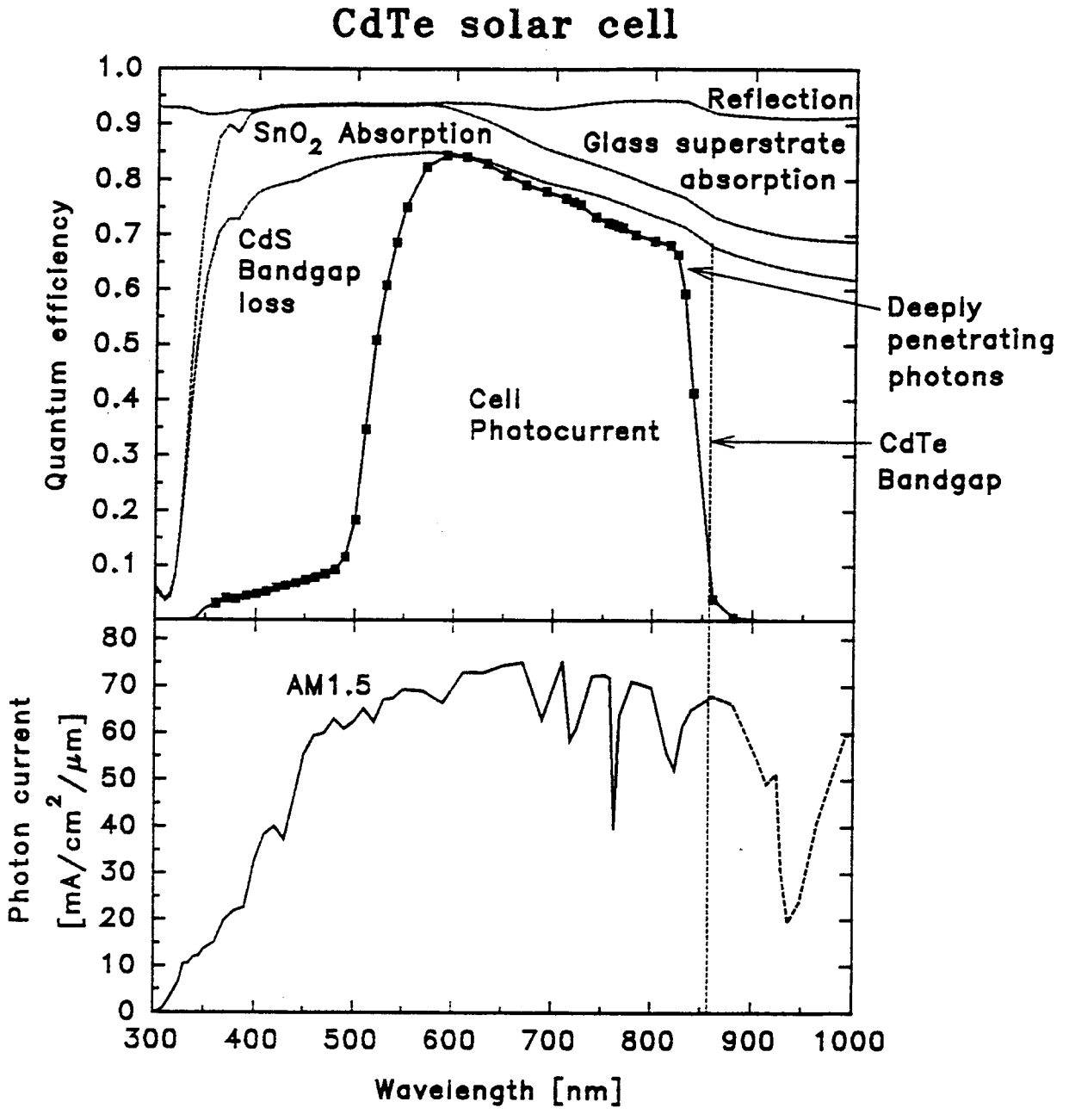


| $J_{sc}$ | Reflection loss | Glass absorp. | $SnO_2$ absorp. | CdS loss | Deep penetr. | Max. photo current |
|---|---|---|---|---|---|---|
| 17.6 | 1.7 | 2.0 | 2.4 | 5.8 | 1.1 | 30.6 |

all currents in $mA/cm^2$

**Fig. 8. Quantum efficiency and photon losses (SCI CdTe cell).**

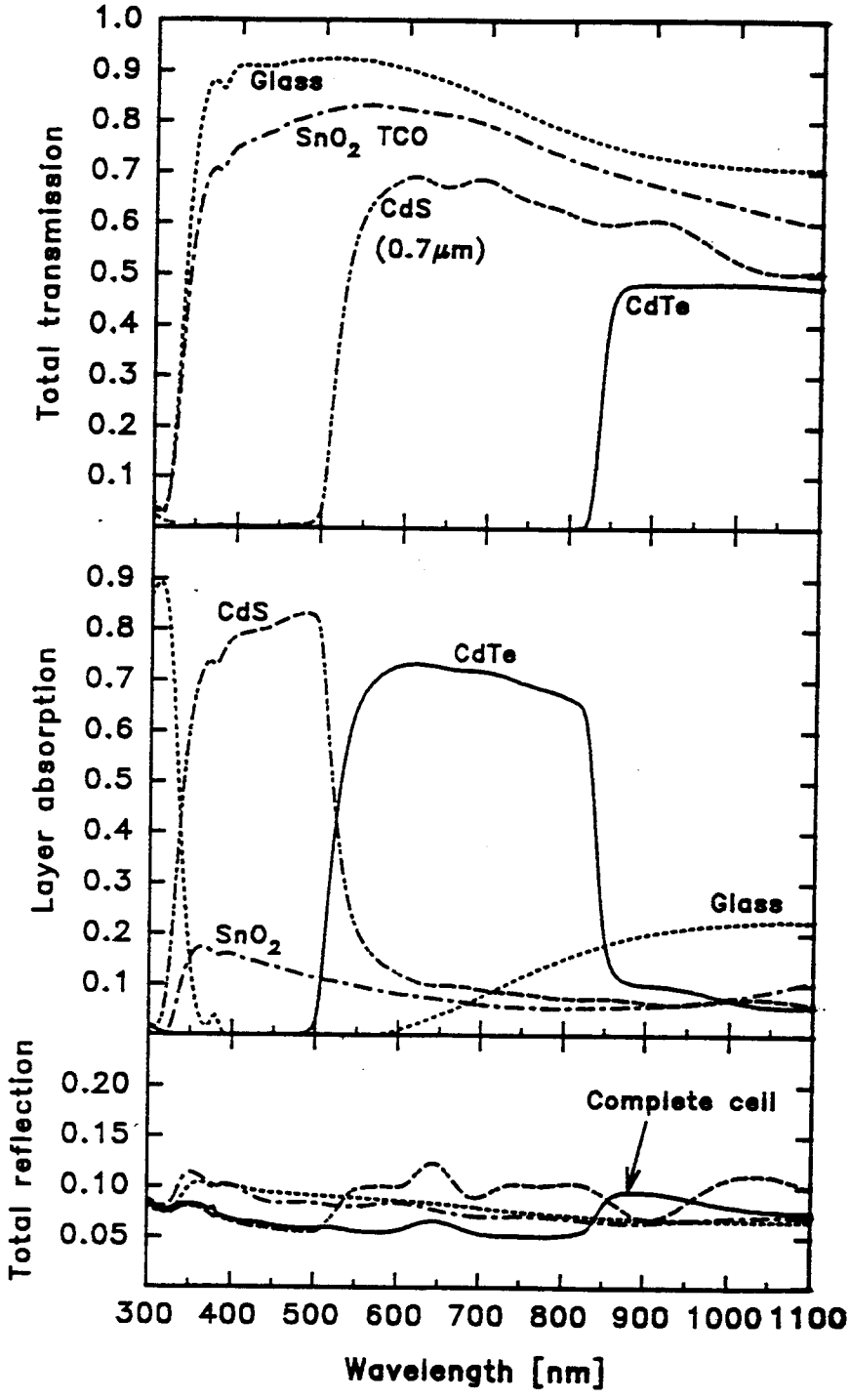


**Fig. 9. Transmission through CdTe cells terminated at four stages (top) supplemented by reflection (bottom) is used to calculate photon absorption in each layer (middle).**

## CdS Thickness

One of the CdTe-cell phonon losses, absorption by the CdS window, has been explored in some depth, again as part of the National CdTe R & D Team. Cells were provided by NREL, U. Toledo (UT), SCI, U. South Florida (USF), Colorado School of Mines (CSM), Institute for Energy Conversion (IEC), and Golden Photon (formerly Photon Energy). In each case, varying thicknesses of CdS were used. Altogether these thicknesses ranged from less than 200 Å up to 3000 Å. An important goal was to investigate how thin could the CdS be, or could it be eliminated altogether, without degrading cell performance.

Fig. 10 shows the QE curves for UT cells of different CdS thickness deposited on Corning 7039 glass (top) and LOF soda-lime glass (bottom). As expected thinner CdS led to higher QE at wavelengths corresponding to photon energies above the CdS bandgap (See Publ. 14).

The photocurrent due to the short-wavelength photons, those with wavelengths less than 520 nm, are plotted as a function of CdS thickness in Fig. 11 for cells made by UT and the other labs listed above. These photocurrent are roughly exponential in thickness. They cover a range from approximately 2 to 7 mA/cm$^2$, which might correspond to the difference between 10 and 12½% cells.

The 400-Å QE curve in the bottom part of Fig. 10 appears to be lower than the others in the 600 to 800 nm wavelength range, displaying what was referred to in the previous section as an unknown loss. More significant changes in thin-CdS cells, however, are seen in voltage and fill-factor as shown in Fig. 12. Since it is now realized that the thickness of CdS is reduced somewhat during the subsequent CdTe deposition, the x-axis in Fig. 12 was chosen to be the average short-wavelength CdS absorption. Its 0-100% range corresponds to a photon loss of 0-8 mA/cm$^2$. 40% on this scale corresponds roughly to a CdS thickness of 100 Å.

Fig. 12 shows that fill-factor and voltage generally decrease when CdS is thinner. Not shown, however, is a more recent Golden Photon (GPI) cell that maintained its fill-factor and voltage even when the short-wavelength absorption was reduced to essentially zero. Quite likely this cell had a significant mixed layer of $CdTe_{1-x}S_x$.

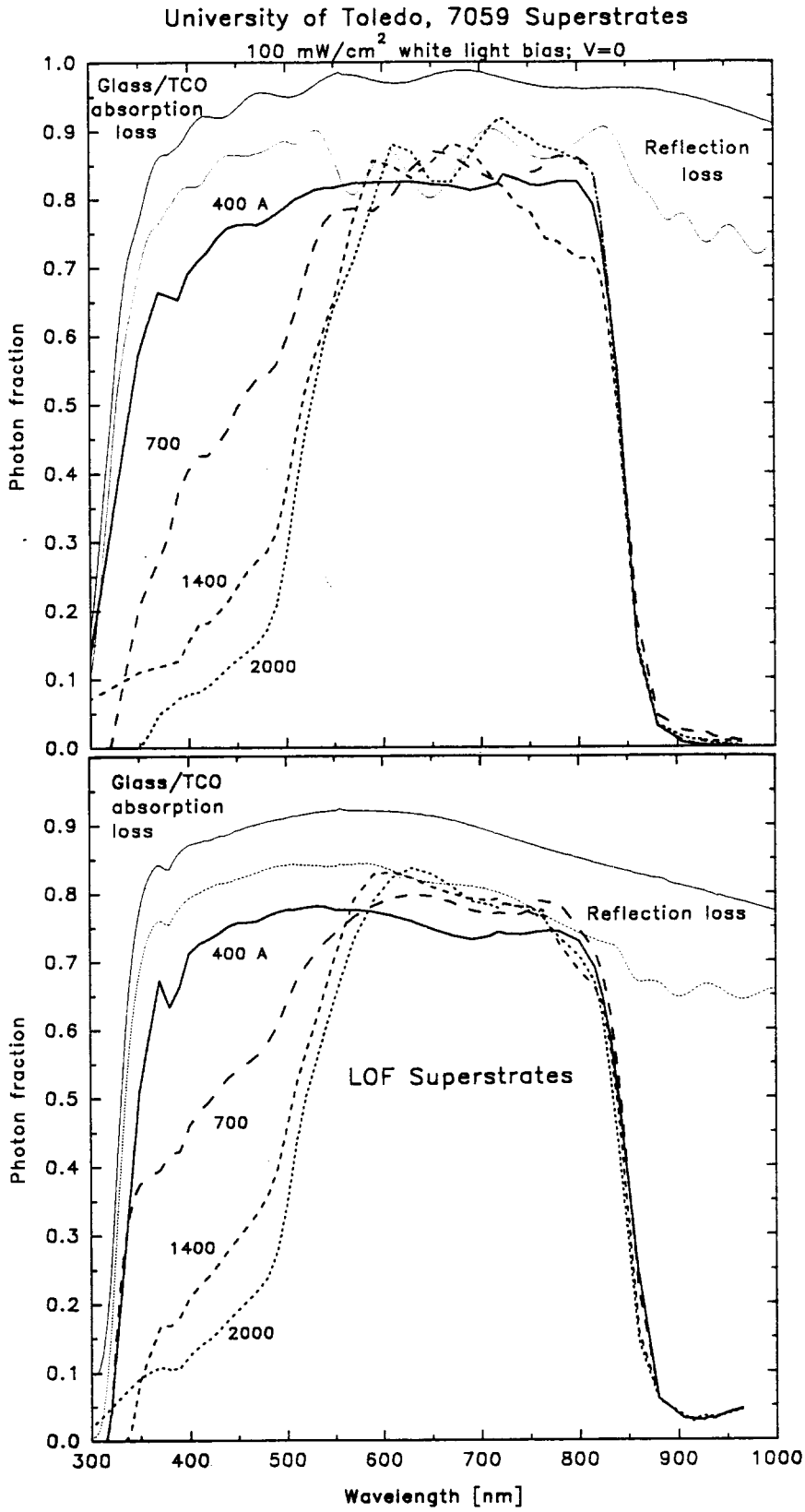


**Fig. 10.** **Quantum efficiency curves for different CdS thicknesses (University of Toledo CdTe cells).**

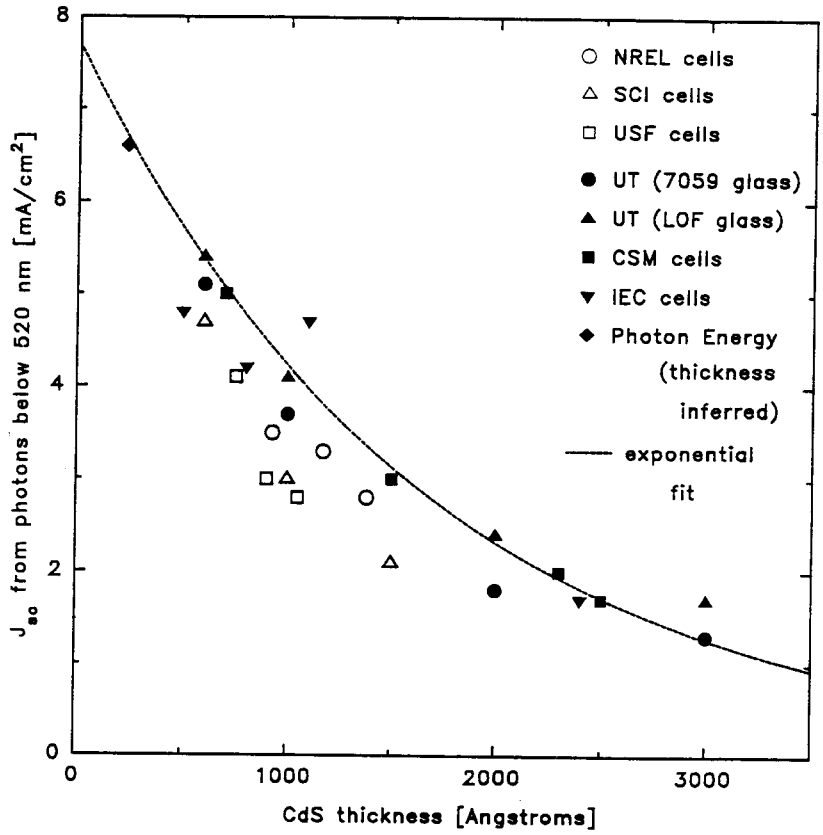


**Fig. 11. Variation with CdS thickness of photocurrent due to short-wavelength photons.**

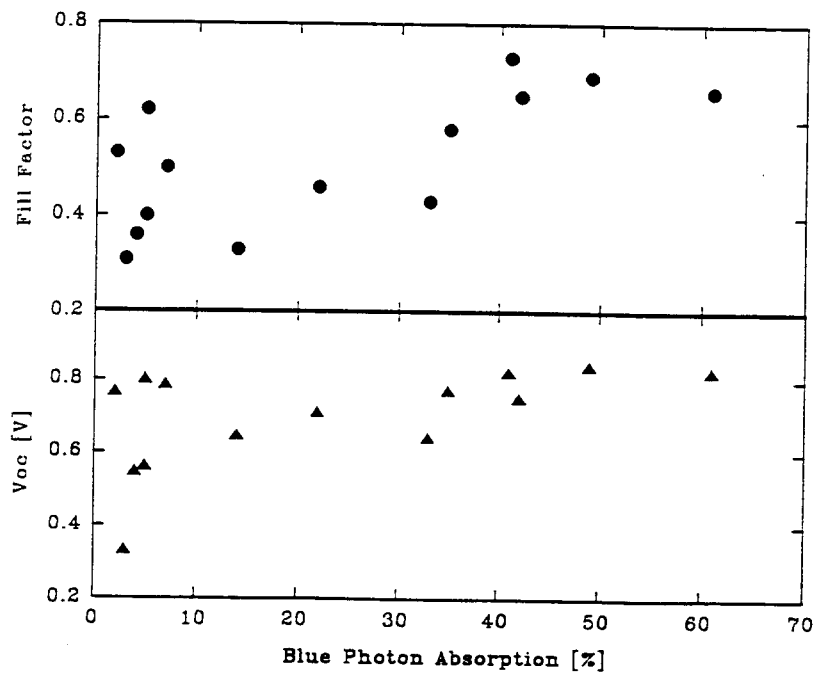


**Fig. 12.** **CdTe cell voltage and fill-factor as a function of short-wavelength CdS absorption (cells from seven laboratories).**

The high-efficiency GPI cell noted above in fact had an efficiency very similar to record-efficiency cells made earlier at USF. It is instructive to compare the current-voltage curves, which is done in Figure 13. At the top, one can see that the GPI cell has a higher current, but lower voltages as one would expect if its effective bandgap were smaller. Its slightly lower efficiency is due to a higher series resistance, and hence, reduced fill-factor. The lower part of Figure 13 shows the band gap cutoff of the QE's on an expanded scale. Also shown for context are the cutoffs for crystalline GaAs and UT CdTe. The wavelength cutoff is 19 nm larger for the GPI cell than for the USF one. This difference corresponds to a 1.2 $mA/cm^2$ larger photocurrent and a 32 mV smaller voltage, values very similar to the differences shown in Fig. 12.

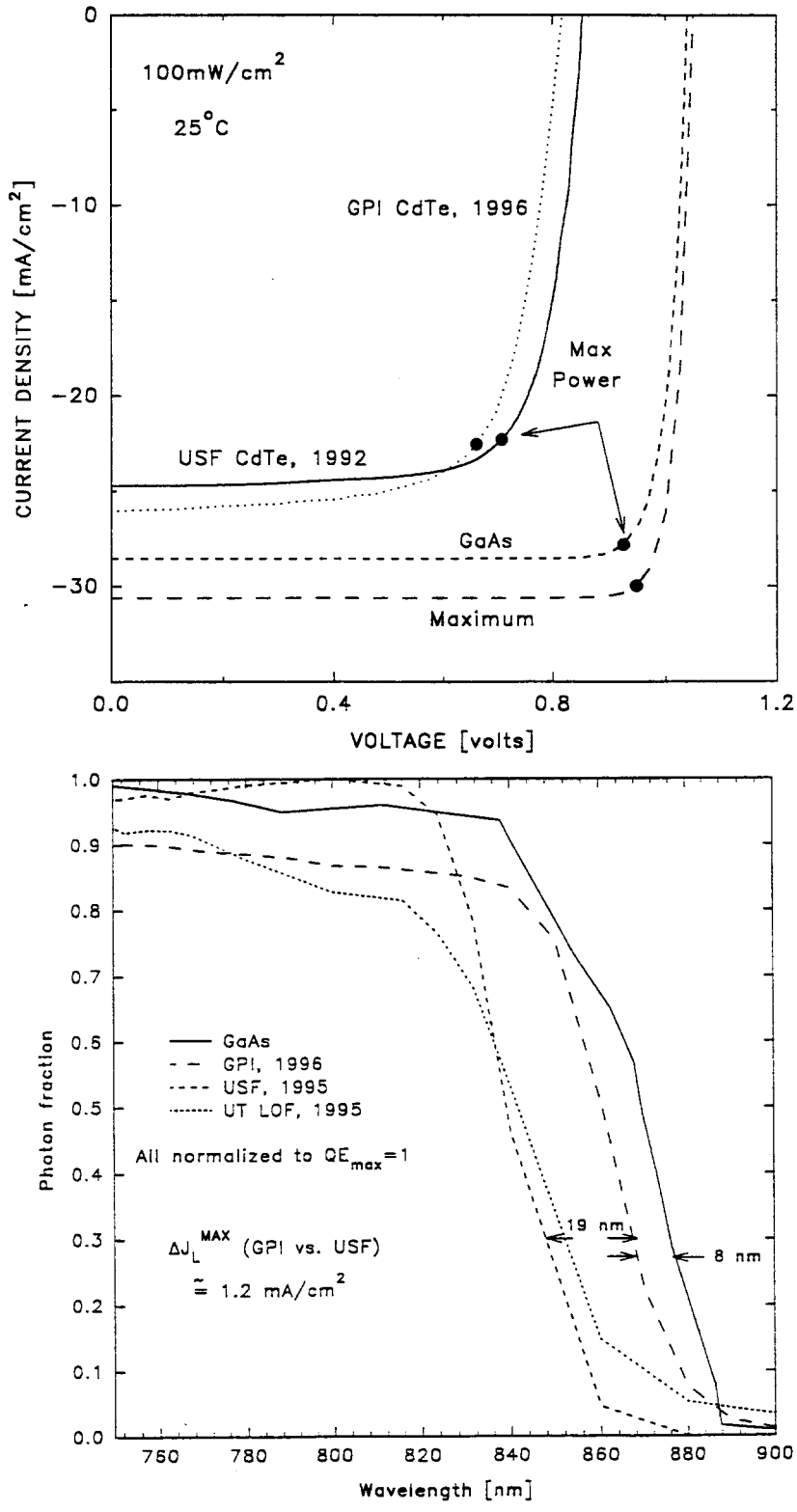


**Fig. 13.** **Comparison of high-efficiency current-voltage curves (top) and quantum efficiency cut-off (bottom) for GPI and USF CdTe cells.**

# CIS/CIGS CELL ANALYSIS

## Sodium Effects

It has been recognized for many years that soda-lime-glass substrates tend to yield better performance CIS cells than borosilicate glass substrates. More recently, several laboratories have demonstrated the positive effect of small amounts of sodium on CIS and CIGS cells. In some cases the sodium diffuses out of the glass into the absorber, and in others, it is deliberately introduced during deposition. There has been conflicting evidence whether the sodium helps by improving the morphology, reducing bulk defects, passivating grain boundaries, or by affecting some other property.

Jennifer Granata has (Publ. 16, 17, and 18) fabricated CIS cells at NREL on several types of substrate (stainless steel, alumina, borosilicate glass, soda-lime glass, and soda-lime glass plus an $SiO_2$ sodium-diffusion barrier) with different amounts of $Na_2$ Se added during the absorber deposition. Inductively-coupled plasma spectroscopy is used to quantify the average sodium concentration at higher levels, and secondary-ion mass spectrometry (SIMS) is used for smaller concentrations and to find the spatial sodium profile. Scanning electron microscopy is used to compare morphologies.

The primary objective of the sodium addition project has been to correlate the amount and location of sodium in CIS and CIGS with cell performance. Sometimes the sodium effect is not completely unambiguous, since it is superimposed on other cell-to-cell variations. Nevertheless, there are several observations that seem to be generally true. Fig. 14 shows $V_{oc}$ and fill-factor for several CIS and CIGS cells. The cells on soda-lime-glass (SLG) substrates had base levels of sodium, i.e. when none was added during deposition, of 0.1 (A), 0.1 (B), and 0.001atomic per cent (C) as deduced from SIMS. Cells on alumina had no detectable base level. The cells with little or no base sodium (circles and diamonds) had lower voltages and fill factor when no sodium was added, but the difference decreased as increasing amounts of sodium were added. For large amounts of sodium ($\lesssim$ 1%), the absorber layer starts to lose adhesion and performance deteriorates rapidly.

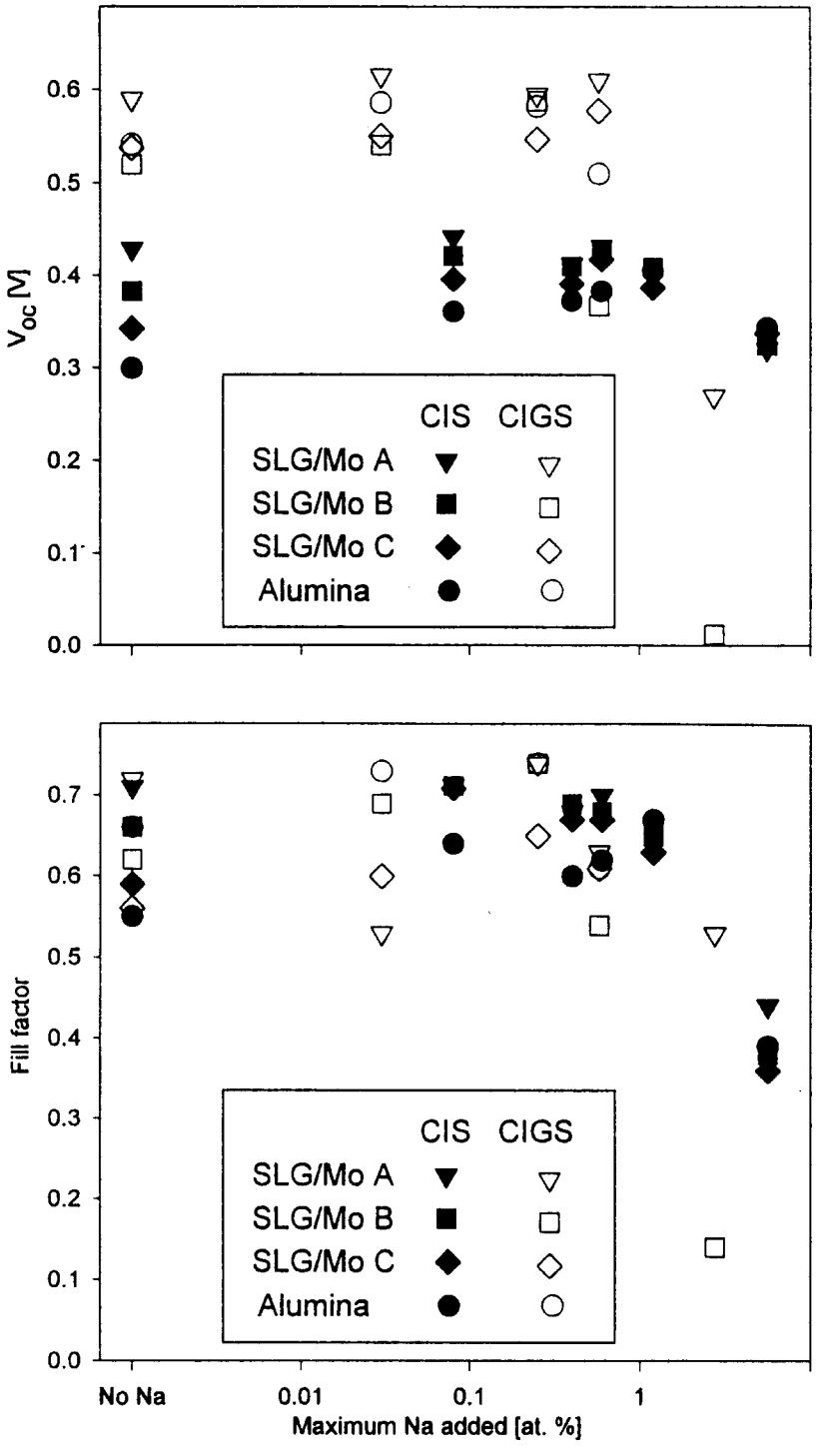


**Fig. 14. Variation in votage and fill-factor with sodium addition for nominally identical cells fabricated on four substrates.**

Based on the current voltage curves, we estimate that the optimal amount of sodium in CIS or CIGS is between 0.05 and 0.5 atomic percent and that over a fairly broad range, the amount makes little difference to performance. Capacitance measurement indicate that the absorber hole density is higher when some sodium is present, which is consistent with the higher voltages. SIMS profiles show that the sodium tends to be more concentrated within 0.5 μm of the surface.

We believe that the most likely reason that sodium improves performance is that it changes the energetics for the primary defect formation. In our view, the basic-principles calculations of Zunger and colleagues are correct that the primary bulk CIS defect is two copper vacancies coupled with indium on a copper site. We further believe there is a similar defect, though determined with different free energies, is associated with CIS grain boundaries. Most excess indium at these boundaries should be passivated by oxygen, or other column VI species, but reduction in the need for excess indium and passivation leads to still better cells. The obvious problem is to calculate, or otherwise deduce, how the defect formation is altered when there is partial substitution of sodium for copper.

**Band-Offset Effects**

Another long standing issue for CIS cells has been the impact of a possible CdS/CIS band offset on cell performance. This impact can be calculated, and Xiaoxiang Liu has evaluated a large number of possibilities using the ADEPT software developed at Purdue University. In general (Publ. 8), there is a broad range of offsets that have only a minor impact on current-voltage curves.

Fig. 15 (top) shows the variation in efficiency with CdS/CIS conduction-band offset assuming typical high-efficiency CIS cell parameters. At room temperature, the efficiency is relatively flat between an offset of -0.4 eV (Type II) and +0.4 eV (Type I). The bottom part of Fig. 15 shows

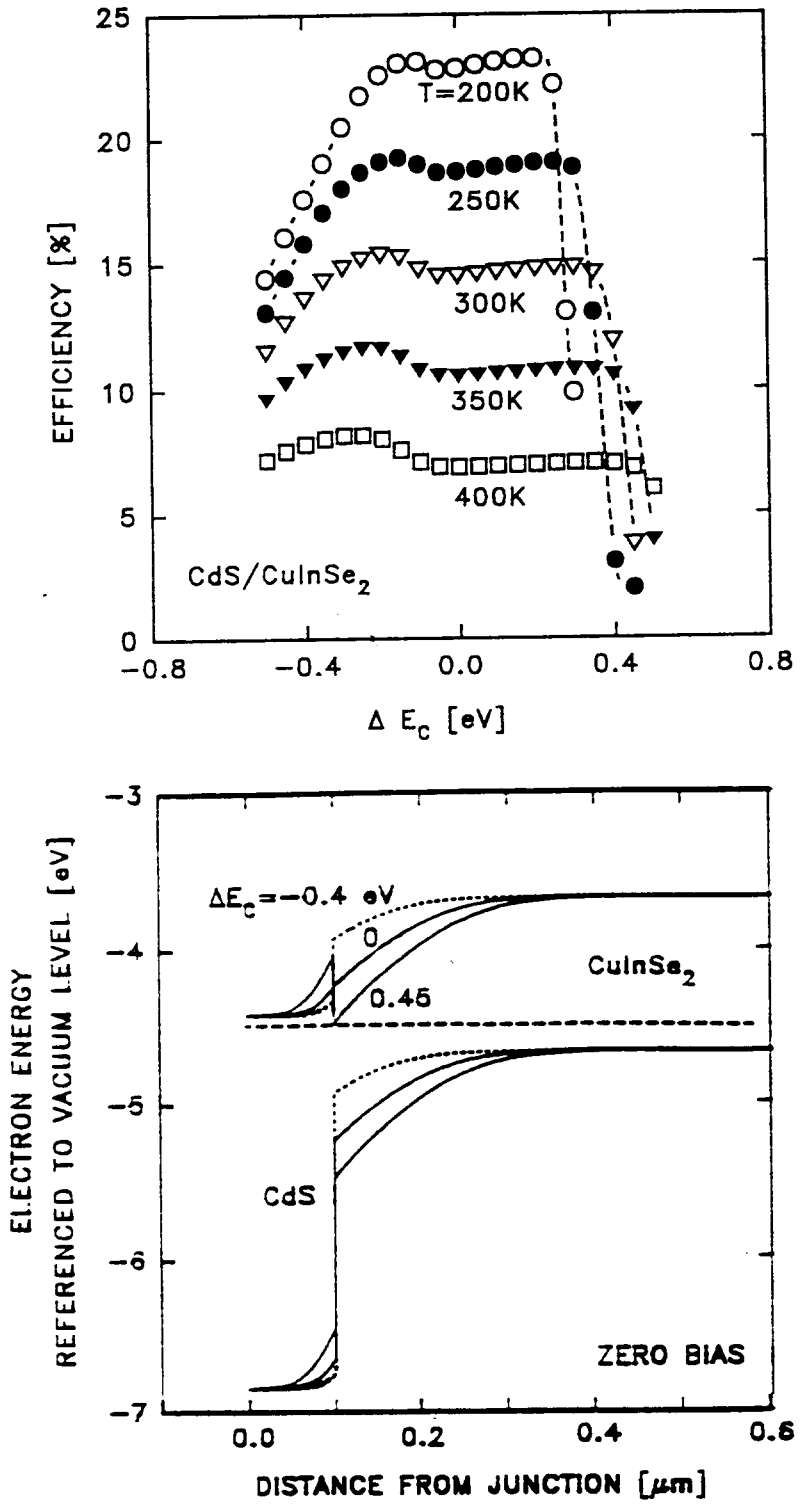


**Fig. 15. Calculated dependence of CIS efficiency on conduction-band offset (top) and corresponding band structure (bottom). Positive offsets mean Type I.**

the differences in band structure for negative, zero, and positive offsets. Inclusion of a thin In-rich CIS surface layer has only a minor impact on those results. The conclusion is similar to that for CdTe back contacts described in an earlier section: unless a secondary barrier is fairly substantial, it has little effect on cell performance. As the top of Fig. 15 indicates, however, the offset that can be tolerated is less at reduced temperatures and greater at elevated ones.

Fig. 15 makes the traditional assumption that most depletion, and hence band curvature, takes place in the CIS absorber. An example calculated by Ingrid Eisgruber (Publ. 22) is shown in Fig. 16 (top). The Fig. 16 curve marked $n^-$–CdS is a calculation based on low carrier-concentration material 0.1 μm thick, plus an assumed negative (Type II) conduction-band offset between the transparent ZnO contact and the CdS. In this case, the highest part of the conduction band, especially in forward bias, occurs in the CdS, and there is effectivly a second barrier to electron flow. With increased carrier-density CdS, labeled n, the extra structure has less impact on electron transport. Included in Fig. 16 is the nearly negligible effect of an indium-rich CIS surface layer.

The light and dark J-V curves resulting from the two CdS densities are shown in the bottom part of Fig. 16. Note the major distortion of the light $n^-$–curve, which has the appearance of a light and a dark diode of the same polarity in series. The secondary diode would increase the turn-on voltage in the dark, but not significantly affect $V_{OC}$ in the light. Such curves are not uncommon experimentally. In fact, some cells show a transition from the $n^-$–curves to the n-curves when exposed to light containing blue photons, and subsequent relaxation over several hours when the blue photons are removed (Publ. 22). Other cells retain the distortion, though blue light may lessen it somewhat. There is probably some selectivity in reporting, so that the experimental curves similar to the distorted one in Fig. 16 may be more prevalent than generally realized.

The proposed explanation for an n- to $n^-$– transition, shown in Fig. 17, is a modification of the occupation of deep CdS states. Figure 17a shows n-CdS without deep levels, where the n-type

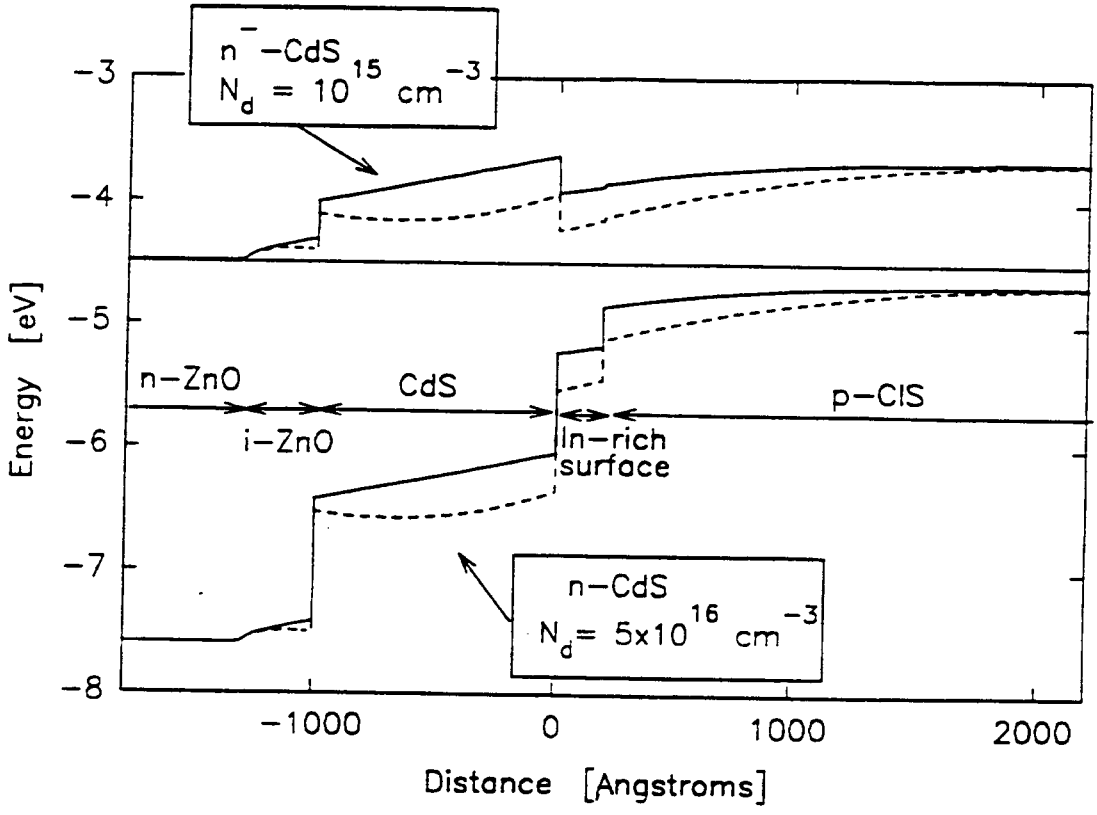


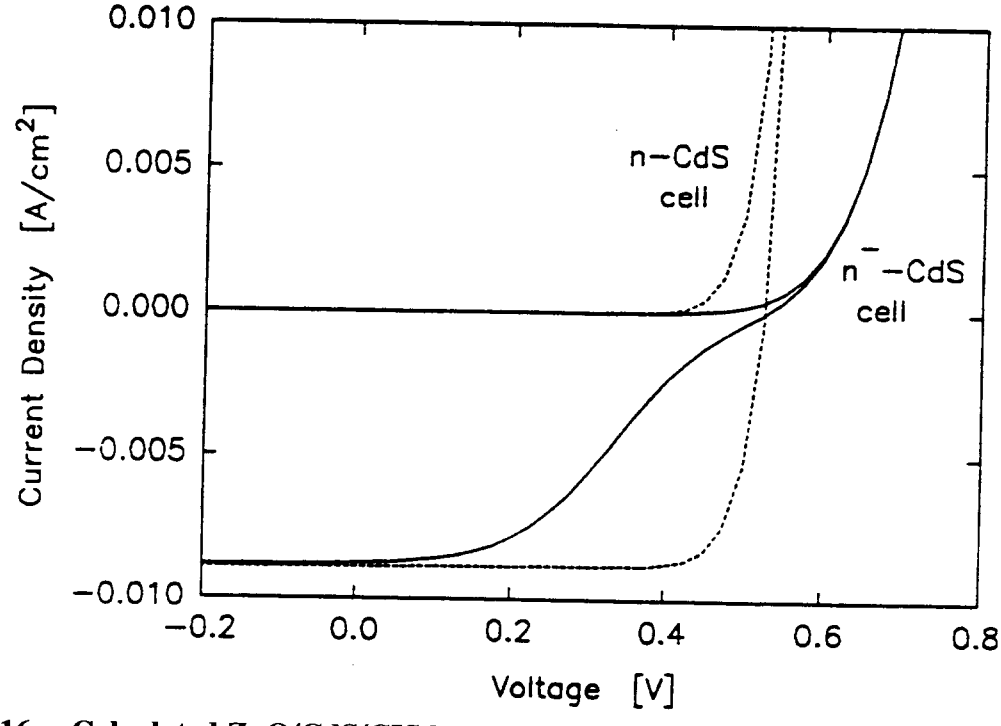


**Fig. 16. Calculated ZnO/CdS/CIS bandstructure contrasting n and $n^-$ CdS (top) and corresponding light and dark J-V curves.**

behavior is due to ionization of shallow donor states. The $n^-$–CdS case is attributed to a density of acceptor-like deep states comparable to the donor density. These deep acceptor states trap most of the free electrons contributed by the donors. The resulting low free electron concentration is shown in Fig. 17b. The effect on the J-V curves will be greatest when the $n^-$–CdS (plus any low-carrier density ZnO) is relatively thick. When incident blue photons are absorbed in the CdS the concentrations of both free electrons and free holes increase greatly, and many of the deep levels are now occupied by light-generated holes, as shown in Fig. 17c. If these deep levels are long-lived, the CdS will remain in the configuration for an extended time, and

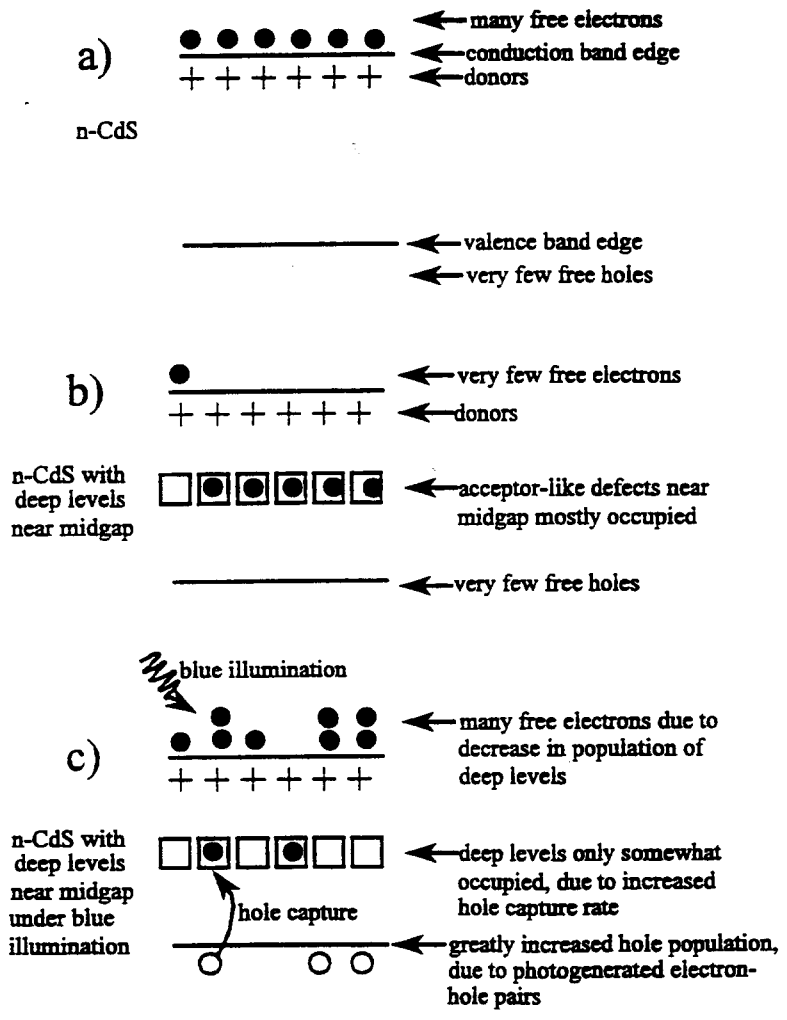


**Fig. 17. Carrier populations in (a) n-type CdS, (b) $n^-$ CdS due to deep levels, and (c) blue illuminations of case (b).**

one will have effectively photoinduced a transition from $n^-$–CdS (few free electrons) to n–CdS (many free electrons). The long relaxation times observed following illumination can be attributed to the slow discharging of the deep traps. Furthermore, the necessity to have photons with energy greater than the CdS bandgap is clearly verified by the separate experiments where longer wavelength light did not affect the $n^-$ curves. If standard light conditions remove the extraneous "$n^-$" features shown in Fig. 16, one might argue that cell performance is not degraded. However, such cells would be located in parameter space close to major performance problems, and it would probably be wise to use information such as Fig. 16 as an indicator of potential trouble.

**Temperature Stress**

Stress tests of CIS cells at elevated temperatures have used the same light and dark facilities described earlier for CdTe cells. The CIS samples studied to date have primarily been fabricated by Siemens Solar Industries (SSI) as part of the National CIS Team effort. They consist of both individual cells and small modules. As with CdTe, the measurements are normally done at room temperature before and after application of elevated temperatures. For this project, the usual elevated temperature was 85° C, and generally samples were first stressed for 20 hours in the dark and then for 20 hours in the light.

Fig. 18 is typical of all the SSI cells and mininodules studied. For consistency, the module data is expressed in terms of the average cell in the module. The pattern is quite clear for both the light and dark measurements. The initial curves (filled circles) are degraded by the dark stress to the open triangle curves. Analysis of the curves shows that the primary change in an increase in series resistance from roughly 1 to 3 $\Omega$-cm$^2$, which of course decreases the fill-factor. The open-circuit voltage is also reduced a small amount, but the diode quality factor and photocurrent are essentially unchanged.

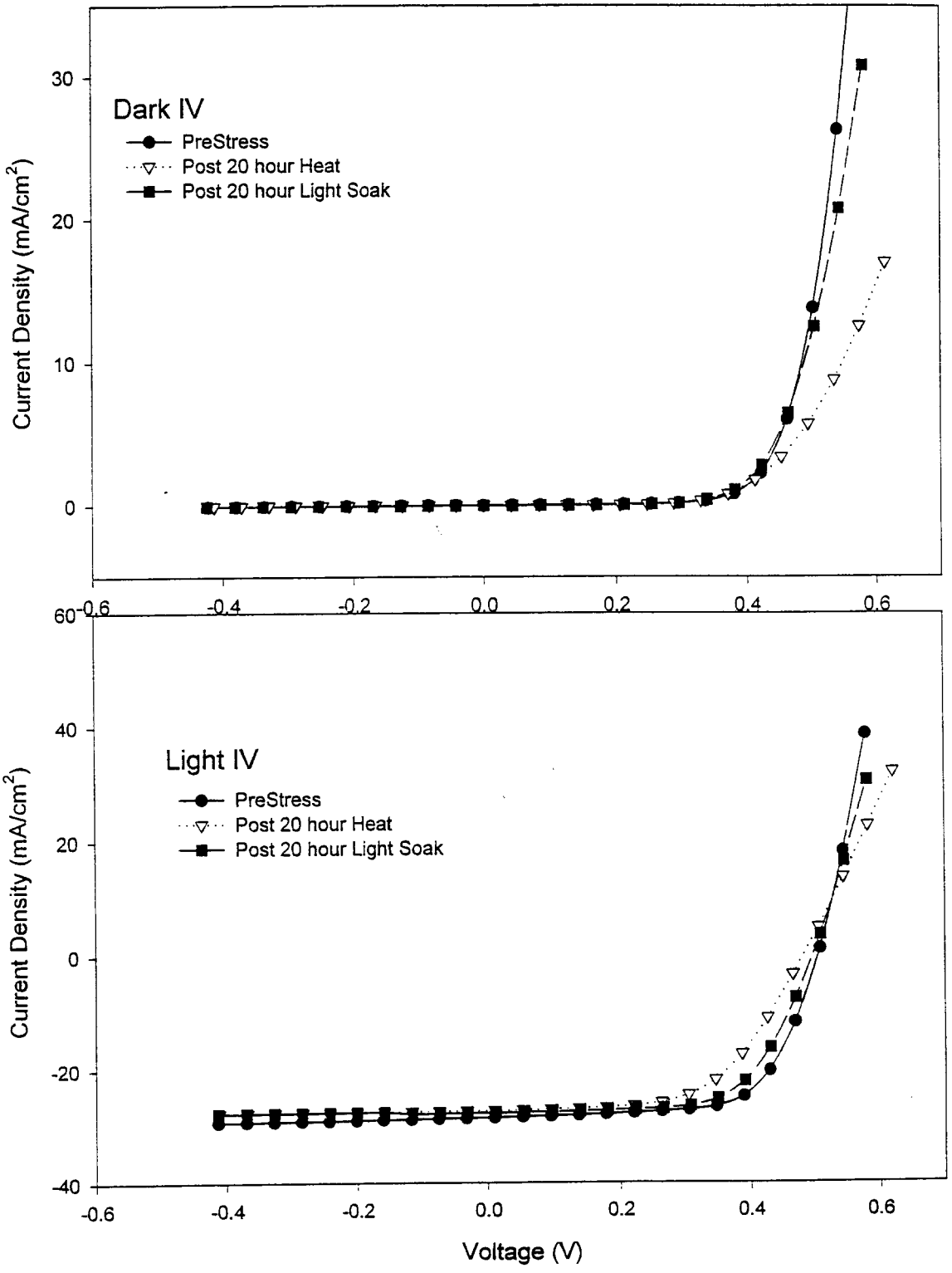


**Fig. 18.** **JV Curves before and after temperature stresses. (SCI-CIS minimodules).**

The next cycle to elevated temperature, this time under illumination of roughly 100 $mW/cm^2$, restores the curves (solid squares) nearly to their original values. Most of the restoration in fact takes place during the first few minutes of illumination. For a pragmatic point of view, this transient behavior is both in the right direction and at least mostly reversible. Qualitatively similar results have been observed in cells from other manufactures.

Capacitance measurements taken at the same time as the current-voltage curves are shown in Fig. 19. In this case also, there is major change during the dark temperature cycle and a near recovery during the illuminated one. The capacitance decreased significantly during the dark cycle meaning an increase in depletion width and a decrease in hold density. The top of Fig. 19 shows $C^{-2}$ vs. V, and the data varies very little with frequency between 10 and 200 kHz. The bottom of the figure converts each point to hole density and depletion width, which is assumed to be primarily in the CIS. The dark cycle lowers the hole density be roughly a factor of three, and the light cycle restores it in approximately the same time frame as the current-voltage curves. In other cases where the initial hole density was somewhat larger than that of Fig. 19, the fractional change, as well as the reduction in voltage, was less than that shown in Figs. 18 and 19.

**Other CIS Measurements**

Three additional CIS projects will be described briefly. The first involved a collaboration with John Kessler at Solarex. In this study the impact of a high-resistivity ZnO layer between the CdS layer and the conducting ZnO front contact. Three cases were compared: A had no high-resistivity ZnO, B had a high-resistivity layer with additional oxygen added during deposition, and C had a high resistive layer deposited without additional oxygen. In each case, different thicknesses of CdS were used corresponding to 0 (no CdS at all), 2, 3, 4, and 8 minutes of chemical-bath deposition (CBD) times. Fig. 20 shows the key solar-cell parameters from one cell per substrate, for the different ZnO conditions and CdS deposition times. The cells with CBD deposition times greater than 2 min have similar parameters and the presence of high-resistivity ZnO does not appear to be significant, though it may reduce shunting somewhat. Quantum efficiency as expected showed less blue response with thicker CdS. All these efficiencies were between the 10 and 12%. With thinner CdS, or none at all, the cells do not perform as well. The 2-min cells had lower voltage and fill factor. In the extreme case, the cells in this study that had neither CdS nor a high-resistivity ZnO layer showed no photovoltaic response.

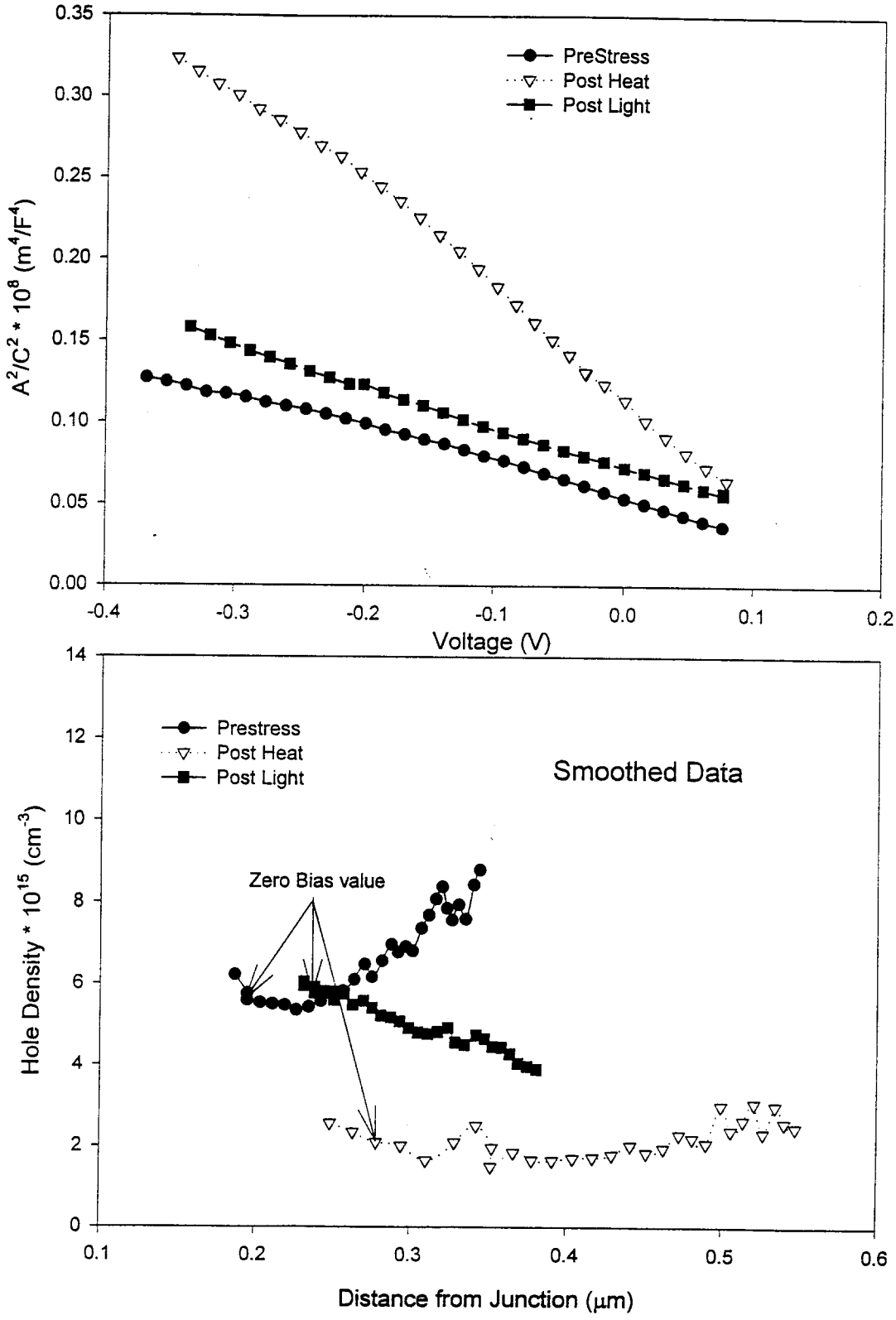


**Fig. 19. Capacitance comparisons before and after temperature stresses. (SCI CIS minimodules).**

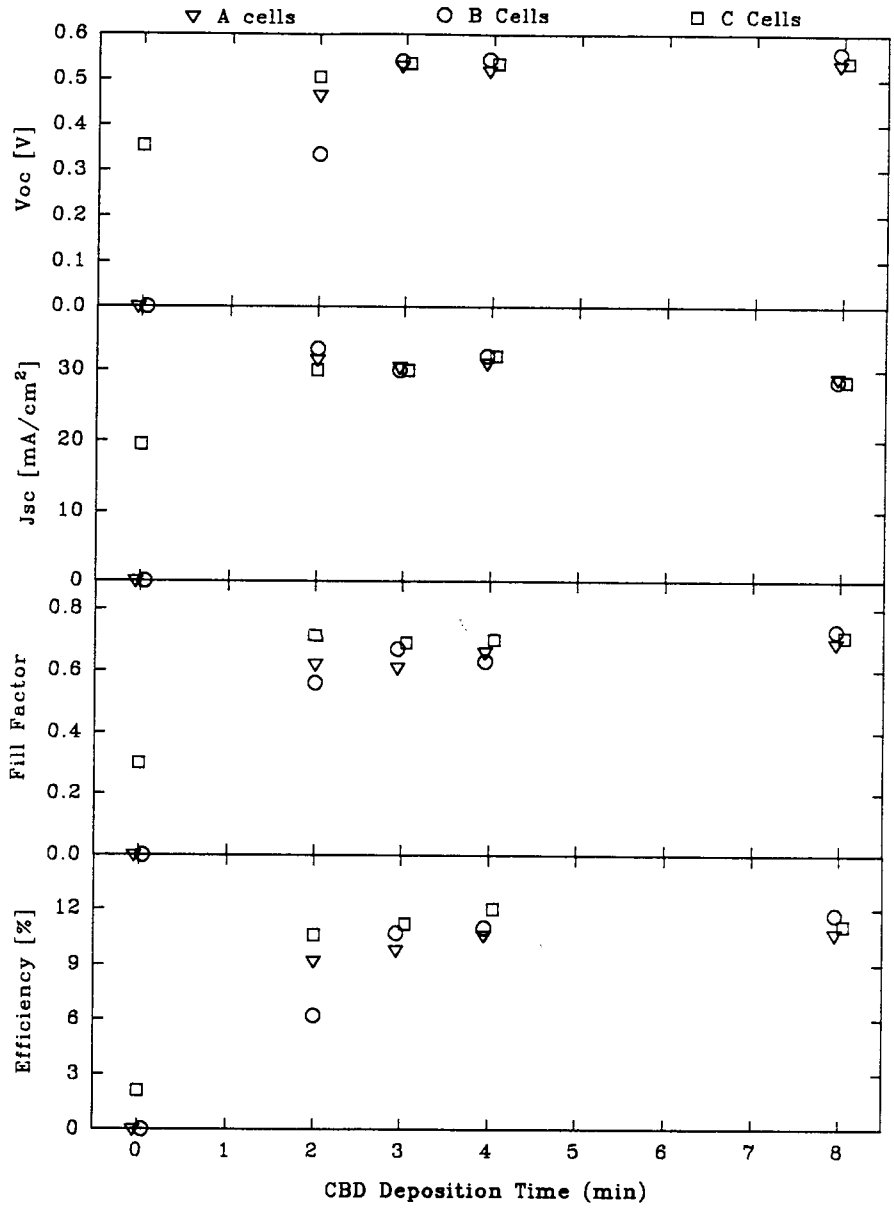


**Fig. 20. Variation in key parameters with deposition time for high-resistivity ZnO buffer layer. (Solarex CIS cells).**

A second additional project was the characterization of CIGS cells fabricated by Raghu Bhattacharya of NREL by electrodeposition (Publ. 20). Three different gallium concentrations were used. Fig. 21 (top) shows the light current-voltage curves for one cell from each concentration. In all cases, efficiencies were in the 12-14% range. Bandgaps deduced from the

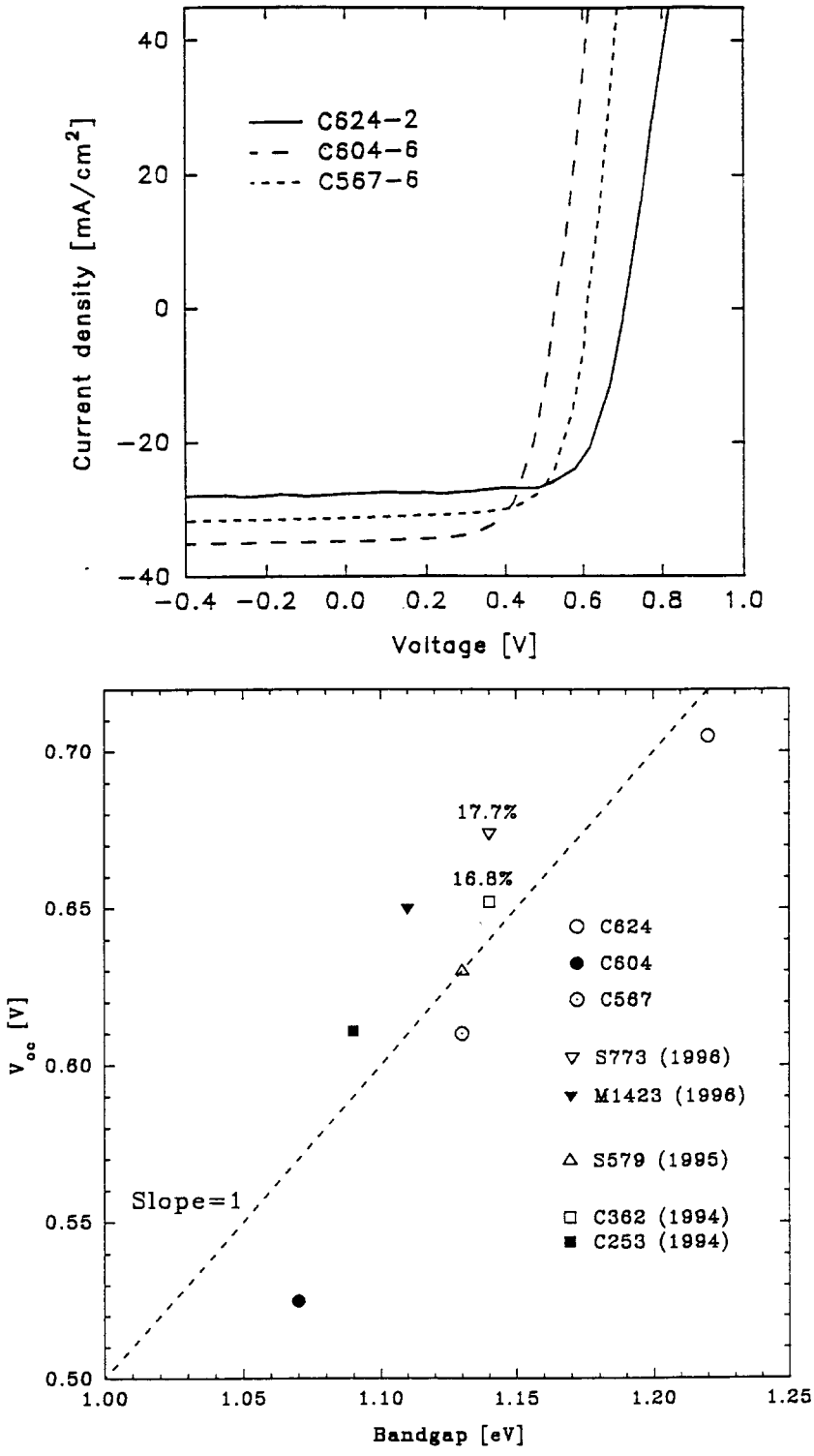


**Fig. 21. Current-voltage curves for electrodeposited cells (top) and variation of $V_{oc}$ with $E_g$ (bottom) (NREL CIGS cells).**

long-wavelength quantum-efficiency cutoffs were 1.07, 1.13, and 1.22 eV for these three cells. The current-voltage curves, which show a progression to higher voltage and smaller current, reflect this variation.

Fig. 21 (bottom) compares open-circuit voltage with bandgap for the three gallium concentrations used for the electrodeposited CIGS cells. The differences between $qV_{oc}$ and $E_g$ are 0.52-0.54 eV. Also shown on the same plot is the progression of record-setting, or near-record-setting. CIGS cells made at NREL by evaporative techniques. The smallest $qV_{oc}$-Eg difference is 0.47 eV. The dashed line is simply an aid to the eye, which corresponds to a difference of 0.5 eV. The results from the electrodeposited CIGS should be viewed as quite good. The 50 mV difference in $V_{oc}$ with the best cells made is remarkable for a technique that has not to date received a large amount of development investment. Particularly noteworthy is the 700 mV cell (open circle) which has a modest $qV_{oc}$-Eg differential at a relatively large gallium concentration.

A third additional study involved record-efficiency CIGS fabricated and measured at NREL. The purpose of this study was to see whether there was any significant difference between the highest-efficiency cells made with the three commonly used NREL deposition systems, referred to internally as S, C, and M. Fig. 22 (top) overlays the current-voltage curves for the best cells from each system. The two cells NREL made in 1996 are about 20 mV higher in open-circuit voltage without an obvious difference in the bandgap of 1.14 eV deduced from the quantum efficiency cutoff. These two cells also have the same current and essentially identical QE curves, which imply an internal quantum efficiency very nearly unity between 550 and 750 nm. The older cell has a QE a few percent lower over this range.

The bottom part of Fig. 22 shows the forward current for the three cells on a logarithmic scale using the same data as the top parts. The fits after removal of the resistive terms are essentially identical for the two newer cells, and the older one is parallel but 20 mV lower in voltage, or equivalently 40% larger in forward current. All three slopes correspond to a diode quality factor of 1.5. Resistive corrections are fairly small: the largest series resistance (S573) reduces efficiency by just over 0.1%, and the smallest shunt resistance (M1574) reduces efficiency by just over 0.2%. In the absence of these resistive losses, all three fill factors would be slgihtly above 0.78.

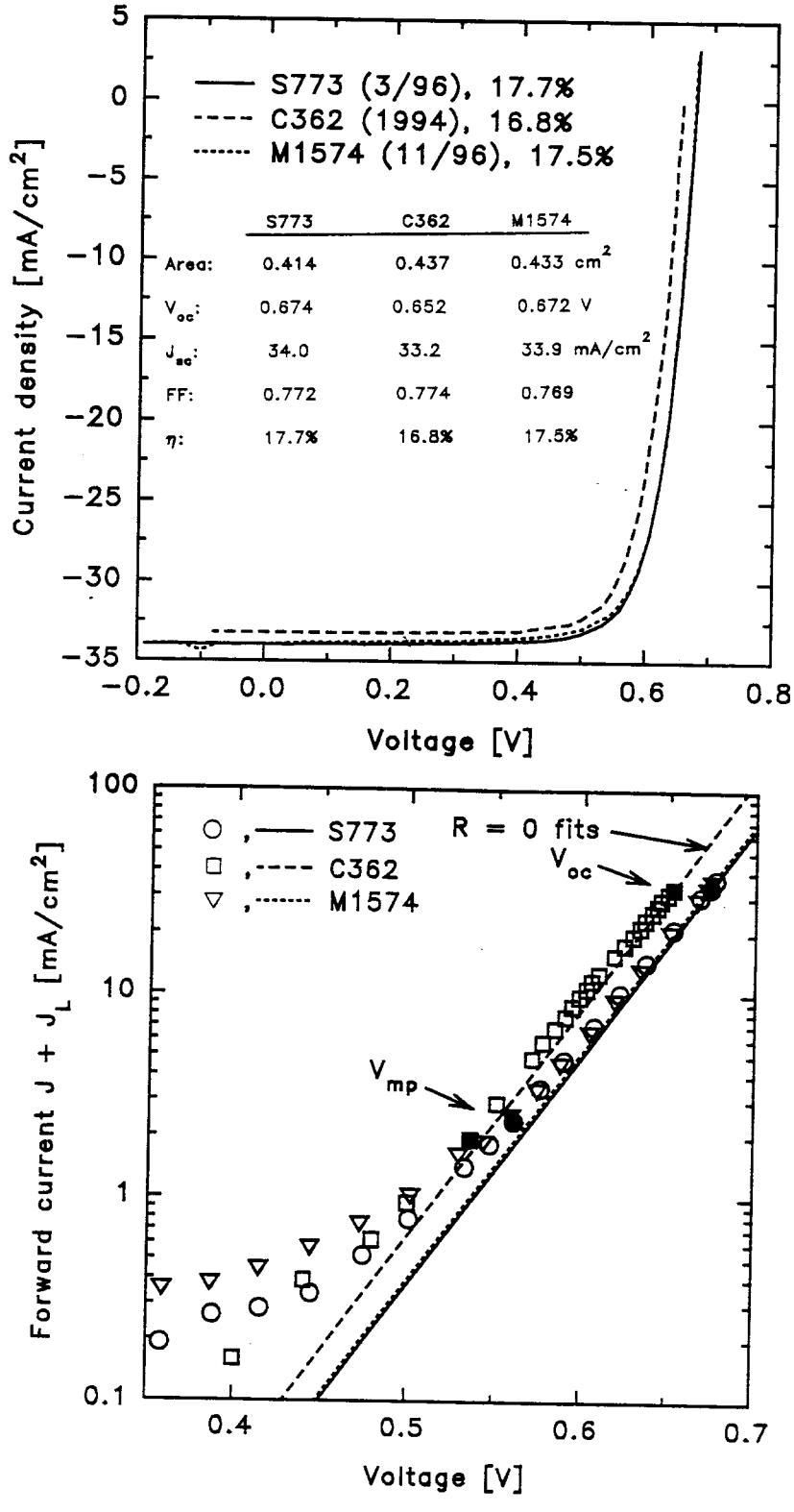


**Fig. 22. Comparison of highest-efficiency NREL CIGS cells on a linear (top) and logarithmic scale.**

# MODULE ANALYSIS

## Cell Geometry

A general, and probably inherent, feature of polycrystalline thin-film module analysis is that the cell geometry is fundamentally different from optimized individual cells or the cells used in crystalline silicon modules (Publ. 5). Essentially all manufactures have focused on a monolithic module consisting of gridless, series-connected cells that are 0.5-1 cm wide (x-direction) and as long (y-direction) as the module (see Fig. 23). This geometry has only a single grid line at the edge of the transparent conductive oxide (TCO) used as the top contact. For the geometries

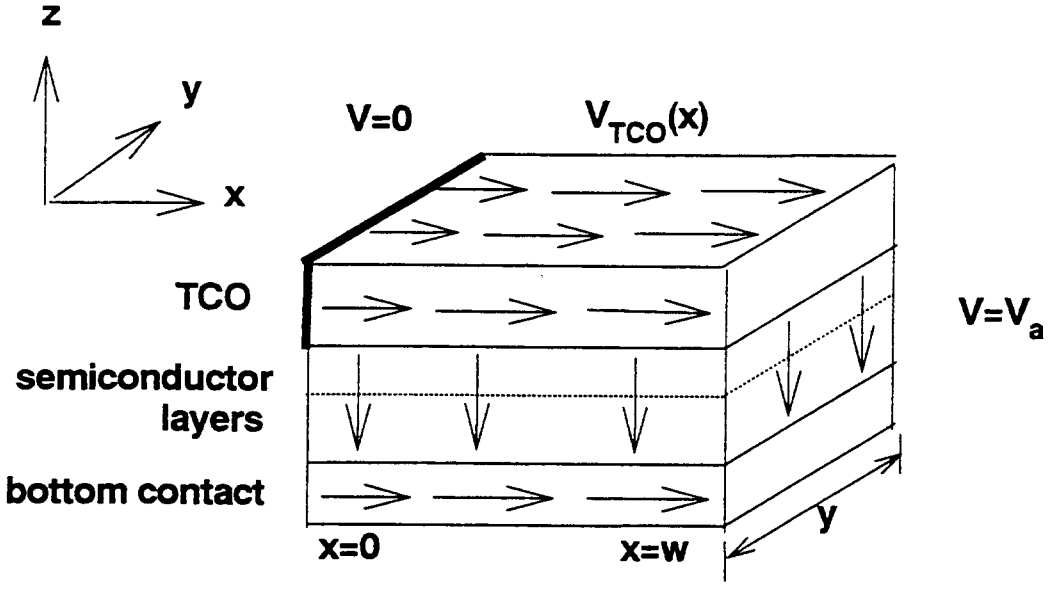


**Fig. 23. Module cell geometry. Thick line shows top contact.**

and TCO layers in current use, the voltage drop across the TCO is 40-100 mV at operating conditions, which corresponds to an effective resistance of 2-5 $\Omega$-cm$^2$. Generally, the voltage drop across the back, or bottom, contact can be assumed to be negligible. Clearly, the measured

current-voltage curve will be distorted if the top surface is probed at a location other than V = O. Even with measurements across the entire cell, however, there are several complications. Figure 24 compares the current-voltage curves for a research-geometry and a module-geometry CdTe cell fabricated under nominally identical conditions. Obviously, there is significant penalty

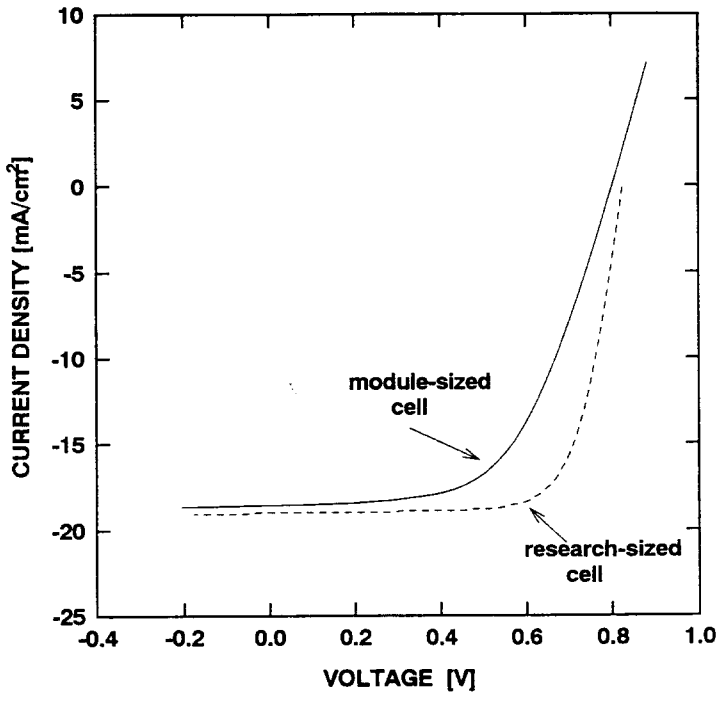


**Fig. 24. Current-voltage curves for research-geometry and module-geometry CdTe cells.**

in fill factor, typically a 10-20% reduction at 100 mW/cm$^2$, but less in the field, since average solar illumination is likely to be closer to 50 mW/cm$^2$. The effective series resistance can be reduced with narrower cells, but at the expense of lost real estate for the additional interconnects. It can also be reduced by a lower sheet-resistivity TCO, but here the usual price is an increase in TCO optical absorption.

Of additional concern for analysis purposes is failure of the single-parameter series-resistance model due to a significant voltage drop across the top contact of each cell. Figure 25 contrasts light and dark J-V curves calculated with a large single-parameter series resistance with those

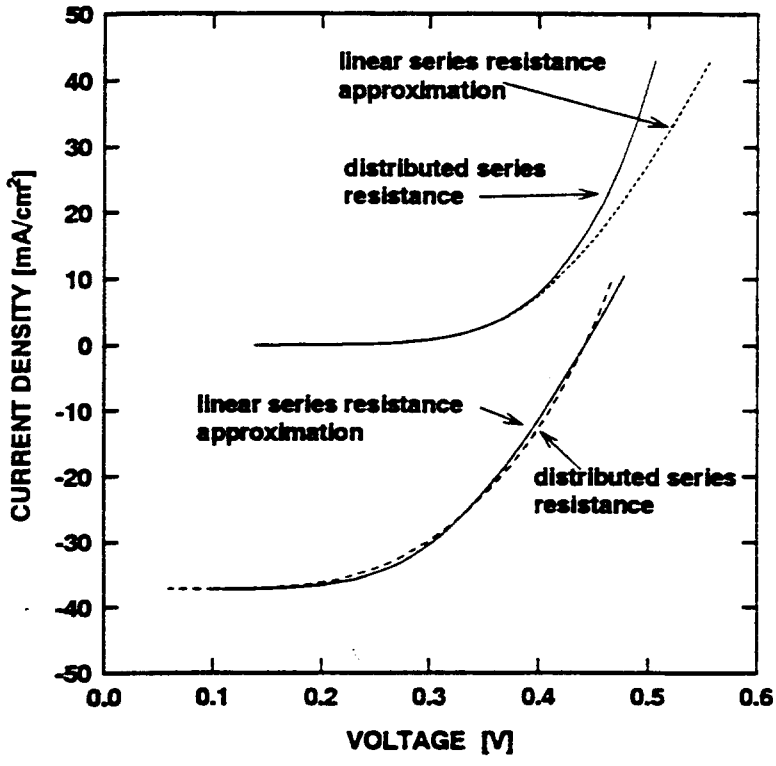


**Fig. 25. Calculated curves for a CIS cell assuming a 1-cm width and a sheet resistance of 7.6 ohms per square.**

calculated more carefully with the proper voltage distribution across the cell. The maximum power point is not much affected, but the diode quality factor is significantly overestimated in the single series-resistance approximation. Subsequent reduction in sheet resistance can therefore by misidentified as an improvement in diode quality factor. Furthermore, the single series-resistance approximation will exaggerate light-dark differences in quality factor and series resistance.

Quantum efficiency measurements on module cells can also give misleading results. For substrate cells, the measurement contacts are typically probes to the TCO layer of adjacent cells. This probe geometry has a load resistant $R_L \sim 10\Omega$. At the same time, the shunt resistance is inversely proportional to cell area, so for a typical shunting of 1000 $\Omega$-cm$^2$, the actual shunt resistance of a 10-cm$^2$ cell is 100 $\Omega$. The measured quantum efficiency ($QE_M$) is related to the actual value (QE) by

$$QE_M = QE/(1 + R_L/R_{sh}) .$$

For the case described, the measured value will be 10% low. For longer module cells, the discrepancy becomes even larger.

## Laser Scanning

Cell-geometry effects will impact all module cells, even if the cells can be contacted individually. In general, however, one may need to test modules where only the two leads to the module are accessible. In this case, laser-scan, or optical-beam-induced-current (OBIC), measurements are appealing, since the light can be easily moved from one cell to another. The work described in the next sections was done by Ingrid Eisgruber with a large-scale laser scanner at NREL (Publ. 2, 6, 12, 15). This apparatus, originally constructed by Rick Matson, is shown in Fig. 26 below. It basically measures the photocurrent induced by a focused beam, typically 25-100 μm in these measurements, that is scanned across in cell or module.

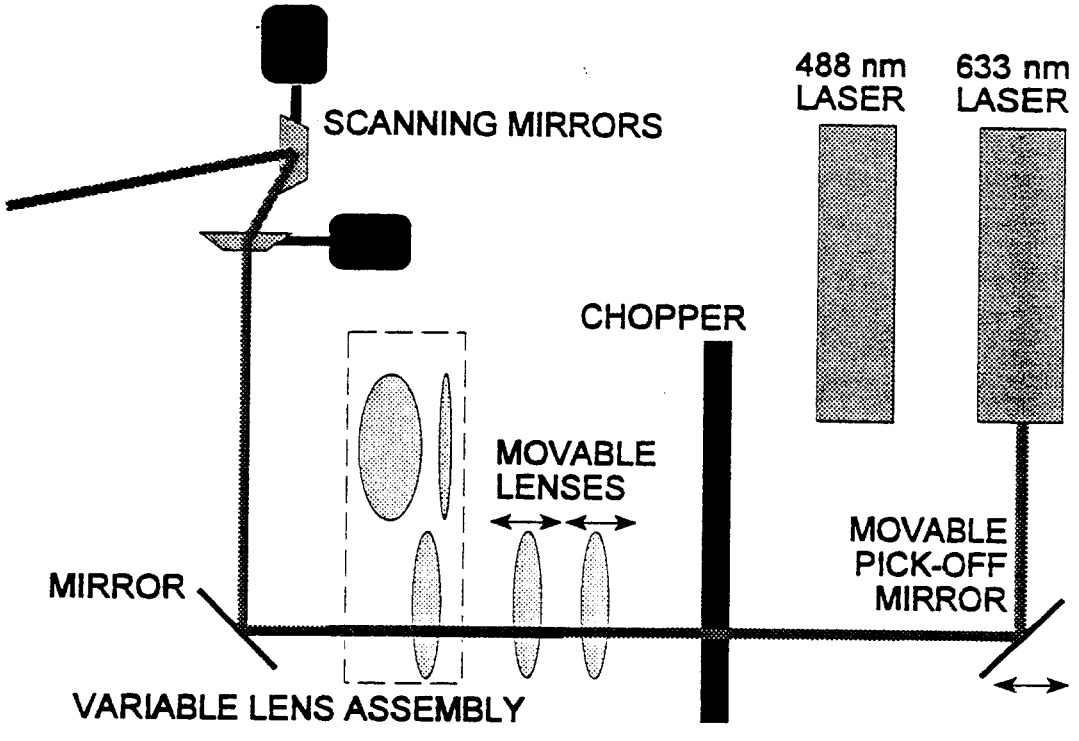


**Fig. 26. Schematic of large-scale laser scanner at NREL.**

## Defect Signatures

A primary use of laser scanning in module analysis is the identification of the location and nature of defects. Cell defects can be loosely divided into local shunts and local areas of reduced

photocurrent. Fig. 27 shows the calculated impact on the photocurrent when the beam passes over 2 μm diameter shunts of varying resistance. The characteristic signature is a gradual decrease in signal over a 1 mm distance scale. Clearly, however, the shunt needs to have a very low resistance to have much impact on the scan. In contrast, a photocurrent defect often yields near-zero signal over the area of the defect and little or no impact elsewhere.

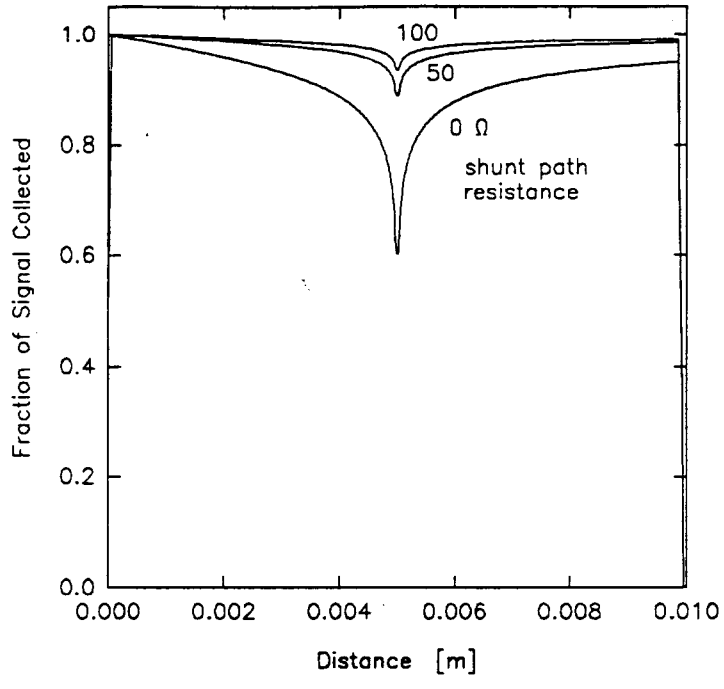


**Fig. 27. Calculated laser-scan signal for a 1 cm wide CdTe cell with a 2μm diameter shunt.**

A combined shunt-photocurrent defect was deliberately introduced to a CIS cell by pricking it with a pin. The resulting shunt resistance was determined to be 1400 Ω (much less of a shunt than any shown in Fig. 27), its diameter was 300 μm, and the transition from full to zero photocurrent was very abrupt. This observation is consistent with the calculation shown in Fig. 28, which shows the effect of the shunt to be negligible compared to the loss of photocurrent. Furthermore, although both are present, the only practical consequence is the local loss of photocurrent.

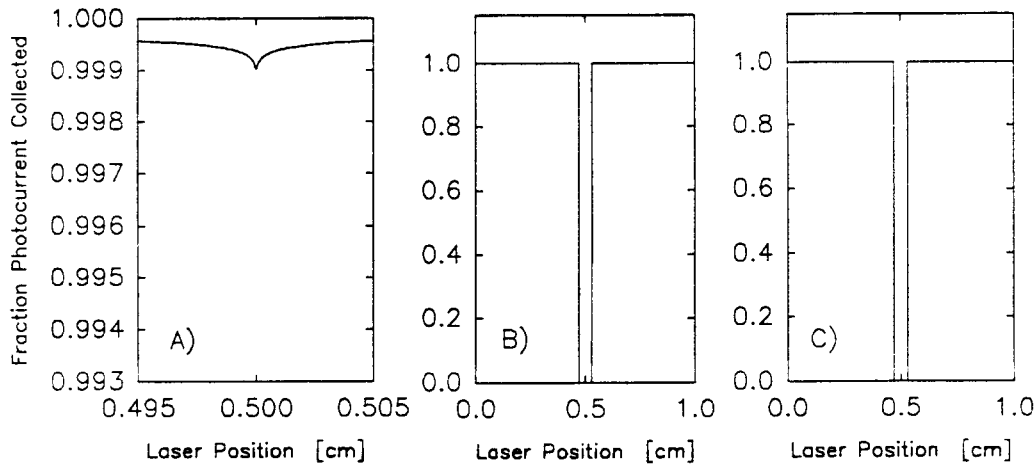


**Fig. 28 Calculated signature of (a) a 1.4 KΩ shunt, (b) a 300 μm photocurrent defect, and (c) a combination of the two.**

## Photocurrent/Shunting Separation

Laser-scanning, or OBIC, measurements can be very valuable in identifying defects in both individual cells and modules. There is a difficulty, however, with analyzing encapsulated modules where the cells cannot easily be contacted individually. At dc or low chopping frequency, the OBIC signal is proportional to the photocurrent/shunt-resistance product. Fig. 29 (top) shows an example where the signal from nominally identical cells in a series-connected module varies greatly. Measurements of the individual cells show that the photocurrents are nearly identical, but there are variations in shunting among the cells. In the high-frequency limit, the photocurrent should be scaled by inverse capacitance, which is generally more uniform than the shunt resistance. Consequently, at higher frequencies (Fig. 29, middle and bottom) the response approaches a value proportional to the photocurrent. Ingrid Eisgruber (Publ. 12) developed a technique to mathematically separate photocurrent and shunt-resistance of encapsulated modules using multiple light-chopping frequencies, even when the highest one is well below the high-frequency limit. This technique was applied to CIGS, CdTe, and a-Si modules, and in each case, the shunt-resistances and quantum efficiency deduced for each cell from the laser scan agreed well with independently measured values.

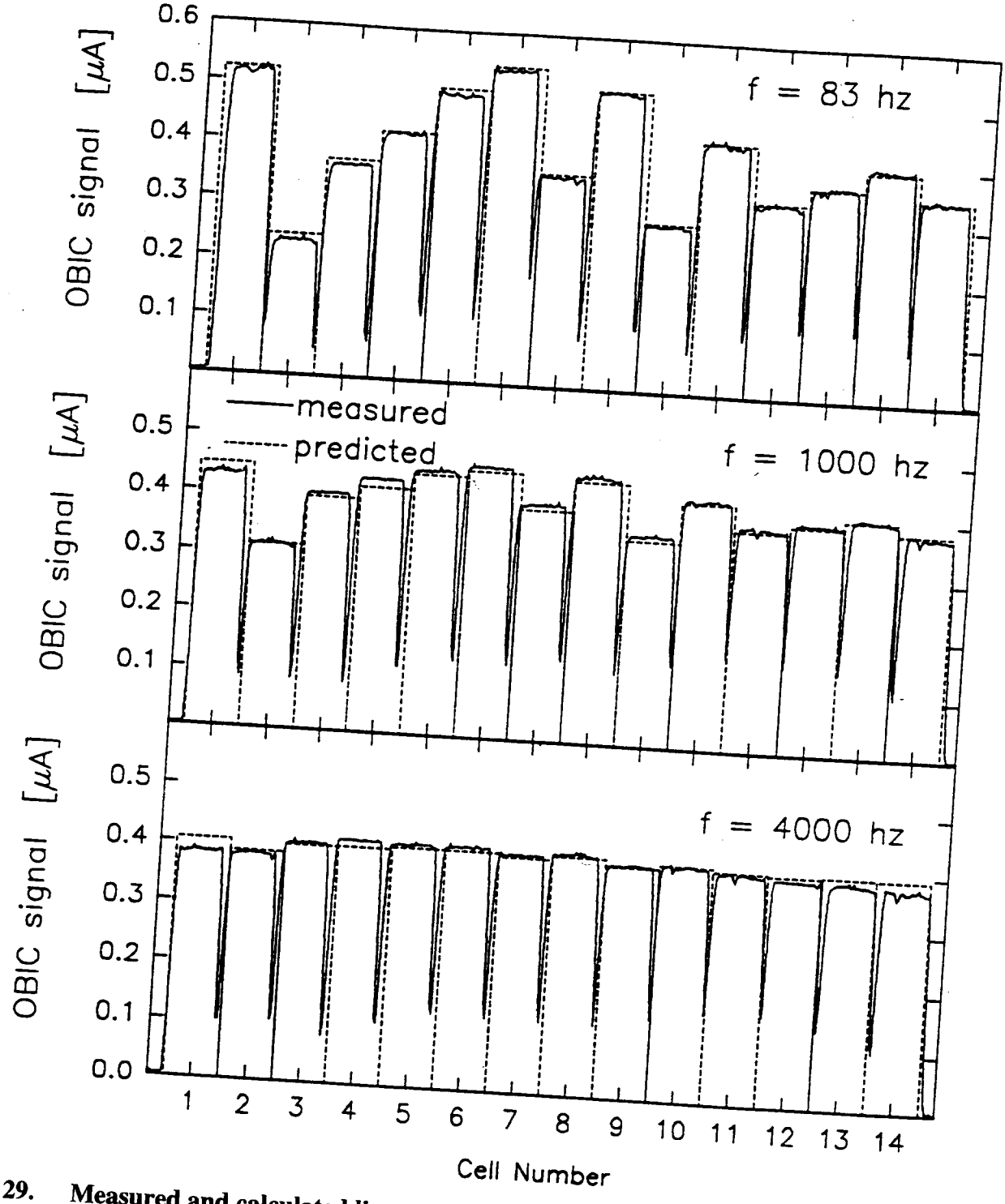


**Fig. 29.** **Measured and calculated line scans at different chopping frequencies for a small CIGS module.**

## Forward Bias/High Intensity

Additional information from laser scanning is available when cells or modules are placed in forward bias or are subjected to sufficient light intensity that they are locally forced into forward bias. Fig. 30 illustrates that variations in series resistance are not observed at zero bias, but are if a cell is forward biased. The apparent quantum efficiency (AQE) is reduced from the zero-bias value by the ratio of the two solid arrows in Fig. 30 and can thus be calculated from the light and dark J-V curves.

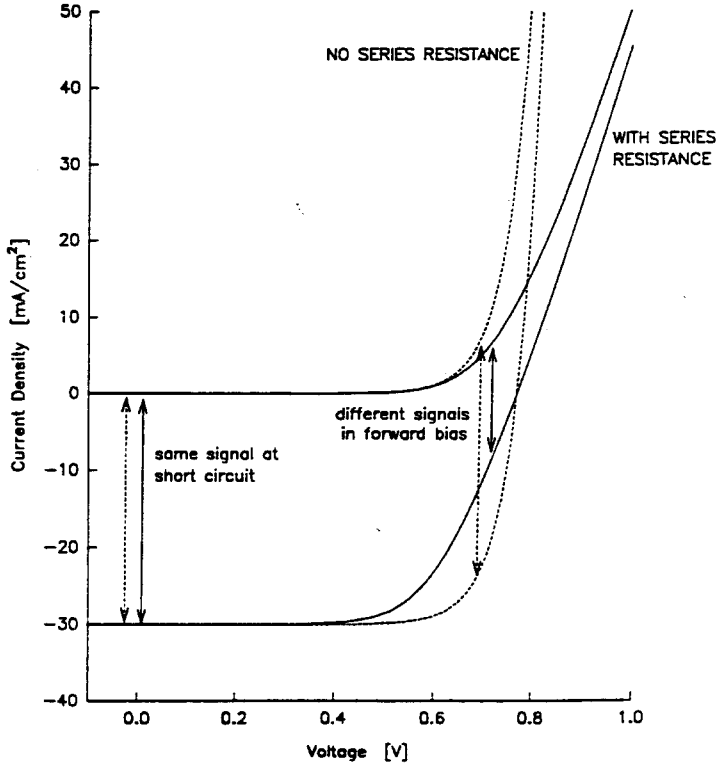


**Fig. 30. Contrast of short-circuit and forward-bias laser scans for cells with and without series resistance.**

Figure 31 shows how AQE varies with series resistance and light intensity for a forward bias between $V_{MP}$ and $V_{OC}$. If other cell parameters are assumed to be fixed, variations in one parameter across the cell can be deduced. Forward-bias scans can therefore be used to identify regions of varying resistivity in $CuInSe_2$ and CdTe cells as shown in Fig. 32. It is necessary to select voltage bias and scan intensity so that the AQE shown in Fig. 31 is relatively sensitive to series resistance.

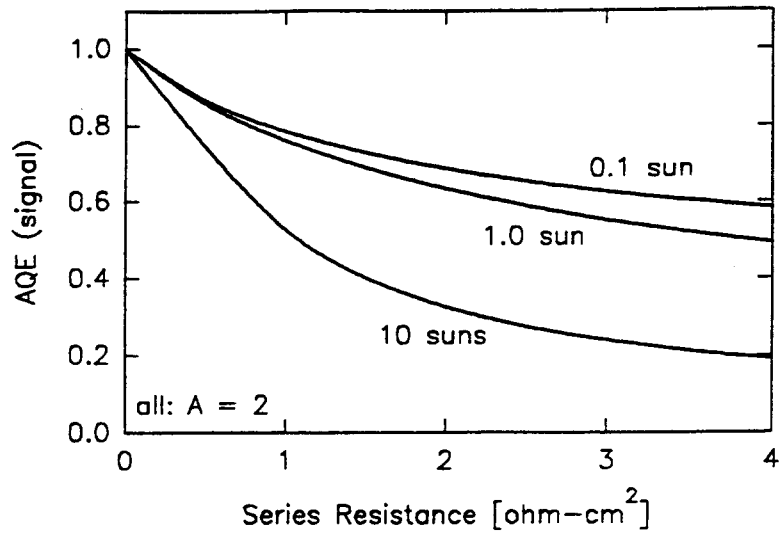


**Fig. 31. Laser-scan signal vs. Series resistance for a typical CdTe cell at 0.74 V forward bias.**

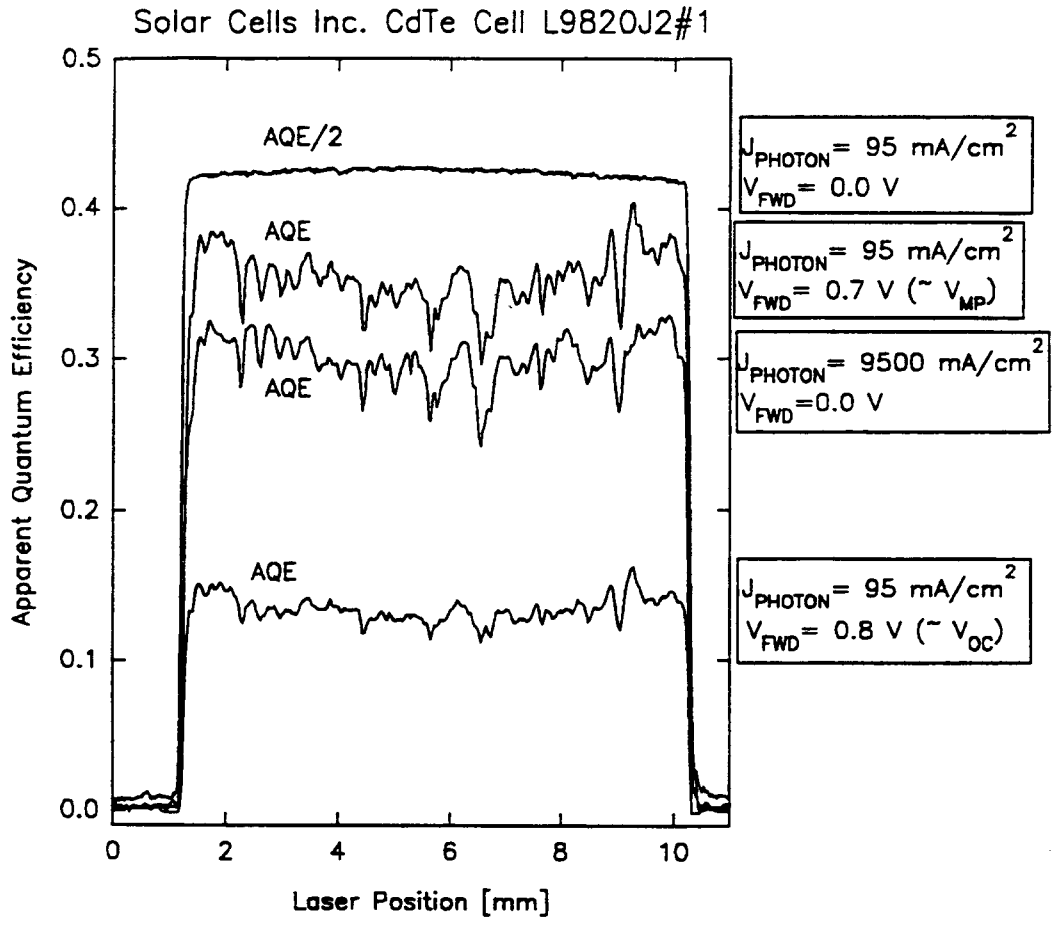


**Fig. 32. Line scans of a CdTe module cell at different voltages and intensities.**

The top scan of Fig. 32 was done at zero bias and a laser intensity comparable to two suns, conditions where AQE is insensitive to series resistance. As expected, it is quite uniform. At forward bias, however, the signal drops by varying amounts depending on the local resistivity. The variations are significantly larger in forward bias or at the higher laser intensities which drive the diode locally into forward bias (9500 $mAcm^2$ trace). Forward bias is also useful for a rough estimate of the leakage in severely shunted cells, where the zero-bias OBIC signal is essentially zero for all accessible frequencies. When bias is increased, however, the leaky cells eventually acquire a signal comparable to the other cells and can be productively analyzed.

# STATUS OF THIN-FILM POLYCRYSTALLINE CELLS

Thin-film polycrystalline solar cells have made remarkable advances in recent years, and in large part these advances can be attributed to becoming more like their crystalline counterparts. Nevertheless, their efficiencies remain significantly below those of crystalline cells of similar bandgap. The highest terrestrial-spectrum efficiency reached by polycrystalline $CuIn_{1-X}Ga_xSe_2$ (CIGS) with a 1.14 eV bandgap $E_g$ is 17.7% [1], compared to 24.0% for 1.12 eV bandgap crystalline Si [2,3]. Polycrystalline CdTe with a bandgap of 1.45 eV has achieved 15.8% [4] compared to 25.7% for crystalline GaAs at 1.43 eV [6]. These differences are shown in the current-voltage curves of Fig. 33, and the numerical values for the key parameters are given in Table II.

We have often (Publ. 1, 3, 7, 11, 23) found it useful to break down the differences between the highest efficiency crystalline and polycrystalline cells into the individual loss mechanisms. The first group of losses, those affecting the photocurrent, can be donev very quantitatively, as described in an earlier section. These losses, which are summarized in Table III, include:

(1) Grid coverage. Superstrate CdTe cells do not commonly have grids, so grid loss is only an issue for CIGS cells. The highest-efficiency CIGS cell had 4% coverage. Furthermore, CIGS modules typically omit metallic grids at some sacrifice in series resistance, so there has been little incentive to reduce the grid area on test cells. In any case, the effect of polycrystallinity is indirect in that the rough surface can complicate the grid contact.

---


[1] J.R. Tuttle et.al., Proc. Mat. Research Soc., San Francisco, CA, 486 (1996) 143.

[2] A. Wang, J. Zhao, and M.A. Green, Appl. Phys. Lett. 57 (1990) 602.

[3] J. Zhao, A. Wang, P. Altermatt, and M.A. Green, Appl. Phys. Lett. 66 (1995) 3636.

[4] C. Ferekides, J. Britt, and Y. Ma, Proc. 23rd IEE Photovoltaic Specialists Conf., Louisville, KY, 1993, p. 389.

[5] S.R. Kurtz, J.M. Olson, and A. Kibbler, Proc. 21st IEEE Photovoltaic Specialists Conf., Orlando, FL., 1990, p. 138.

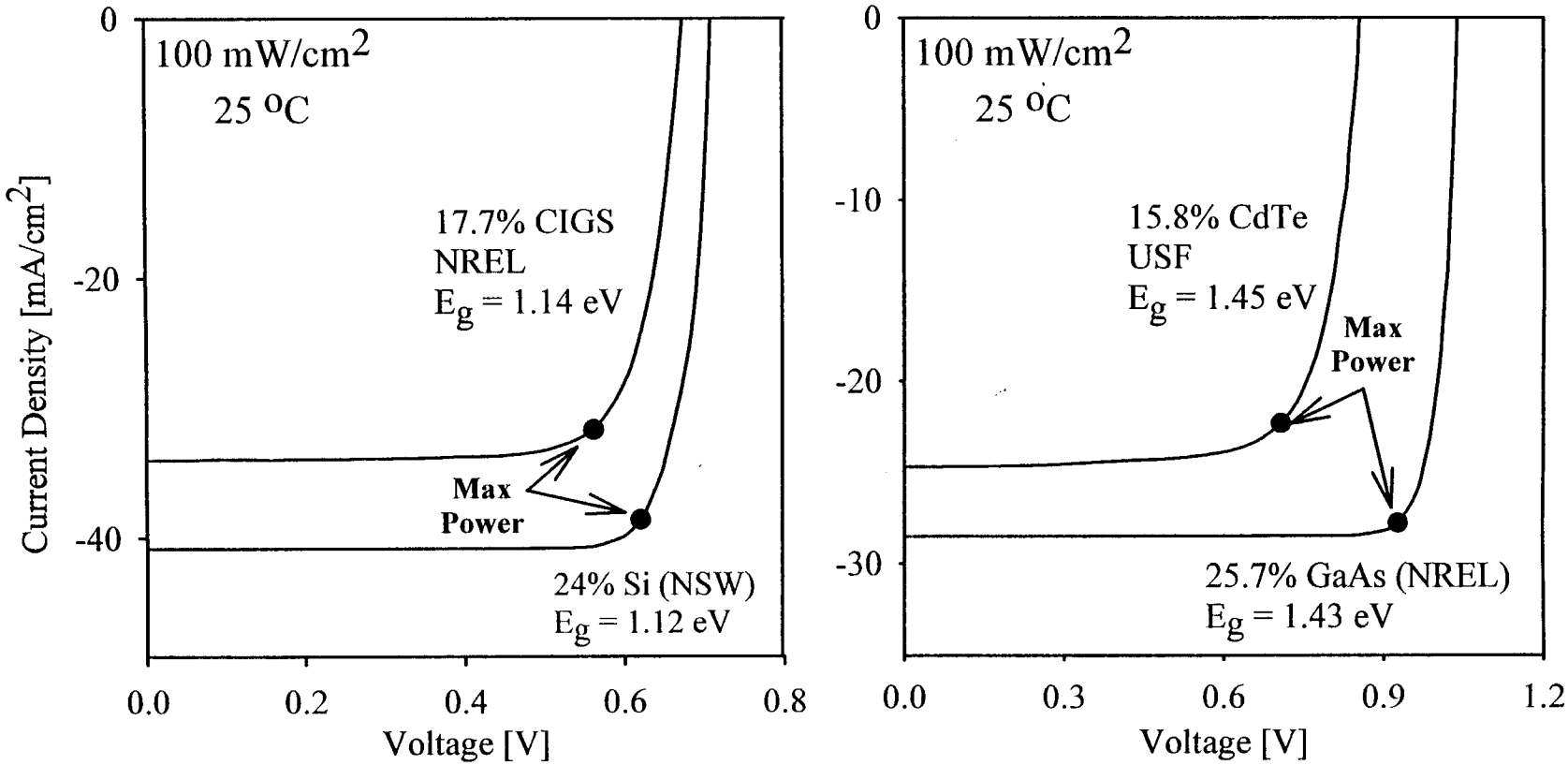


**Fig. 33.** **Highest efficiency current-voltage curves for thin-film polycrystalline solar cells and those for best crystalline cells of similar bandgap. Cells made by the National Renewable Energy Laboratory (NREL), University of New South Wales (NSW) and University of South Florida (USF).**

Table II. Solar cell parameters for the highest efficiency crystalline Si and GaAs, and polycrystalline CIGS and CdTe devices.

| Material | Crystalline Silicon | Polycrystalline $Cu(In,Ga)Se_2$ | Crystalline GaAs | Polycrystalline CdTe |
|---|---|---|---|---|
| $V_{OC}$ [V] | 0.708 | 0.674 | 1.039 | 0.843 |
| $J_{SC}$ [mA/cm$^2$] | 40.8 | 34.0 | 28.5 | 25.1 |
| $V_{mp}$ [V] | 0.620 | 0.560 | 0.930 | 0.705 |
| $J_{mp}$ [mA/cm$^2$] | 38.6 | 31.6 | 27.8 | 22.3 |
| Fill factor | 0.83 | 0.77 | 0.87 | 0.75 |
| Efficiency [%] | 24.0 | 17.7 | 25.7 | 15.8 |
| $r_{shunt}$ [Ω-cm$^2$] | >10000 | 3800 | >10000 | 3500 |
| Diode Quality Factor | 1.0 | 1.6 | 1.0 | 2.2 |
| $R_{series}$ [Ω-cm$^2$] | 0.1 | 0.2 | 0.1 | 0.15 |
| $E_G$ [eV] | 1.12 | 1.14 | 1.43 | 1.45 |

Table III. Excess efficiency losses in the best thin-film polycrystalline cells compared with their crystalline counterparts. The total loss is given, and the portion due to granularity is estimated.

| Loss | Quantity Affected | Aspect of Granularity | CIGS Total | CdTe Total | Due to Granularity |
|---|---|---|---|---|---|
| Grids | Photocurrent | Morphology | 0.9% | 0% | small |
| Reflection | Photocurrent | Morphology | 0.7 | 1.0 | small |
| Window Absorption | Photocurrent | Morphology | 1.2 | 1.3 | small |
| Diffusion Length | Photocurrent | Recombination | 0.7 | 0.2 | nearly all |
| Built-in Potential | Open-circuit Voltage | Compensation | 0.4 | 1.0 | medium |
| Recombination Current | Open-circuit Voltage | Recombination | 0.9 | 3.6 | nearly all |
| | Fill-factor | Recombination | 1.2 | 2.5 | nearly all |
| Series Resistance | Fill-factor | Barriers | 0.2 | 0.1 | small |
| Leakage | Fill-factor | Morphology | 0.1 | 0.2 | nearly all |
| TOTAL | | | 6.3 | 9.9 | |

(2) Reflection. The primary CdTe reflective loss is from the front surface of the glass superstrate. For CIGS it comes from a high index window material often covered by a single-layer antireflection coating. In neither case is the reflective loss a direct consequence of the polycrystallinity, nor has major effort gone into reductions.

(3) Window absorption. Thin-film polycrystalline cell windows generally consist of n-type CdS and a transparent conductive oxide (TCO) contact. For CdTe, a glass superstrate is added. Each of these components absorbs a measurable fraction of the incident photons. Here also, the loss is not directly attributable to the polycrystallinity, but it does appear that the rougher morphology commonly requires thicker CdS and TCO layers.

(4) Diffusion length. The diffusion length in CIGS is considerably reduced by carrier recombination at grain boundaries in the bulk material. The impact on cell performance can be quantified by analysis of the quantum efficiency of long-wavelength photons not absorbed in the high-field depletion region. The impact on CdTe cells is less, since the hole density is generally lower and the depletion regions are consequently thicker.

The open-circuit voltage losses in CIGS and CdTe cells result from two primary causes:

(5) Built-in potential. Carrier density, which can be determined from capacitance measurements, is generally reduced in a polycrystalline cell by grain-boundary states, which partially compensate the majority-carrier holes. Hence, the absorber Fermi level is deeper in the energy gap, and the built-in potential is correspondingly lower. This effect is partially compensated by a reduction in carriers available for conduction at flat band. It is the most difficult of the losses to quantify, but should be less for CIGS, with somewhat higher absorber density, than for CdTe.

(6) Forward recombination current. The largest polycrystalline cell loss results from excess forward current due to recombination of electrons and holes at trapping states in the depletion region of the diode. This loss is clearly due to the polycrystallinity and is particularly large for CdTe cells. This loss can be expressed either as the ratio of forward currents, or more commonly as the voltage difference between cells normalized to the bandgaps.

The excess forward recombination current lowers the fill-factor as well as the open-circuit voltage, since the crystalline-polycrystalline voltage difference at maximum power ($V_{MP}$) is generally larger than that at open-circuit ($V_{oc}$). The reason for the larger difference is that the polycrystalline curves have a weaker knee corresponding to a larger diode quality factor (1.6 for CIGS, 2.2 for CdTe, near 1.0 for Si and GaAs). There are however, two additional fill-factor losses; neither of which generally has a major impact on the high-efficiency cells.

(7) Series resistance. The series resistance is quite small for all the cells shown. For the high-efficiency polycrystalline cells, it is likely due to the TCO layer and probably not significantly affected by transport barriers between grains.
(8) Leakage. The leakage conduction of thin-film polycrystalline cells is generally high, but not sufficiently high to significantly affect the cells' efficiency. The primary leakage is likely due to occasional low resistance paths resulting from the granular structure.

The eight losses discussed above are summarized in Table III. The quantitative breakdown for the excess losses in the highest-efficiency CIGS and CdTe cells is given in columns 4 and 5. The loss values shown are corrected for the small bandgap differences with Si and GaAs respectively. The current and fill-factor breakdowns are quite reliable, but the values assigned to the two voltage losses are more speculative. The proportions of the eight loss factors will vary among high-efficiency cells according to the fabrication techniques employed, but the largest factor in all such cells to date has been the excess recombination current.

Table III shows there is not a clearly dominant loss for CIGS and CdTe solar cells. Fig. 34 shows a graphical comparison with the best crystalline cells, and breaks the differences down into photocurrent, open-circuit voltage, and fill-factor effects. The shaded part, about two thirds of the total difference, represents the losses directly due to polycrystallinity. Thus, there is a need for strategies to further reduce the grain impact. Such strategies might include deliberate incorporation of impurities into the absorber, such as Na in CIGS and Cl in CdTe, or techniques to bring growth processes closer to thermodynamic equilibrium. Other strategies which are not directly affected by the granularity would include CIGS grid-area reduction, more sophisticated

anti-reflection coatings, development of TCO layers with smaller absorption-resistance products, and the thinning or elimination of the CdS layer.

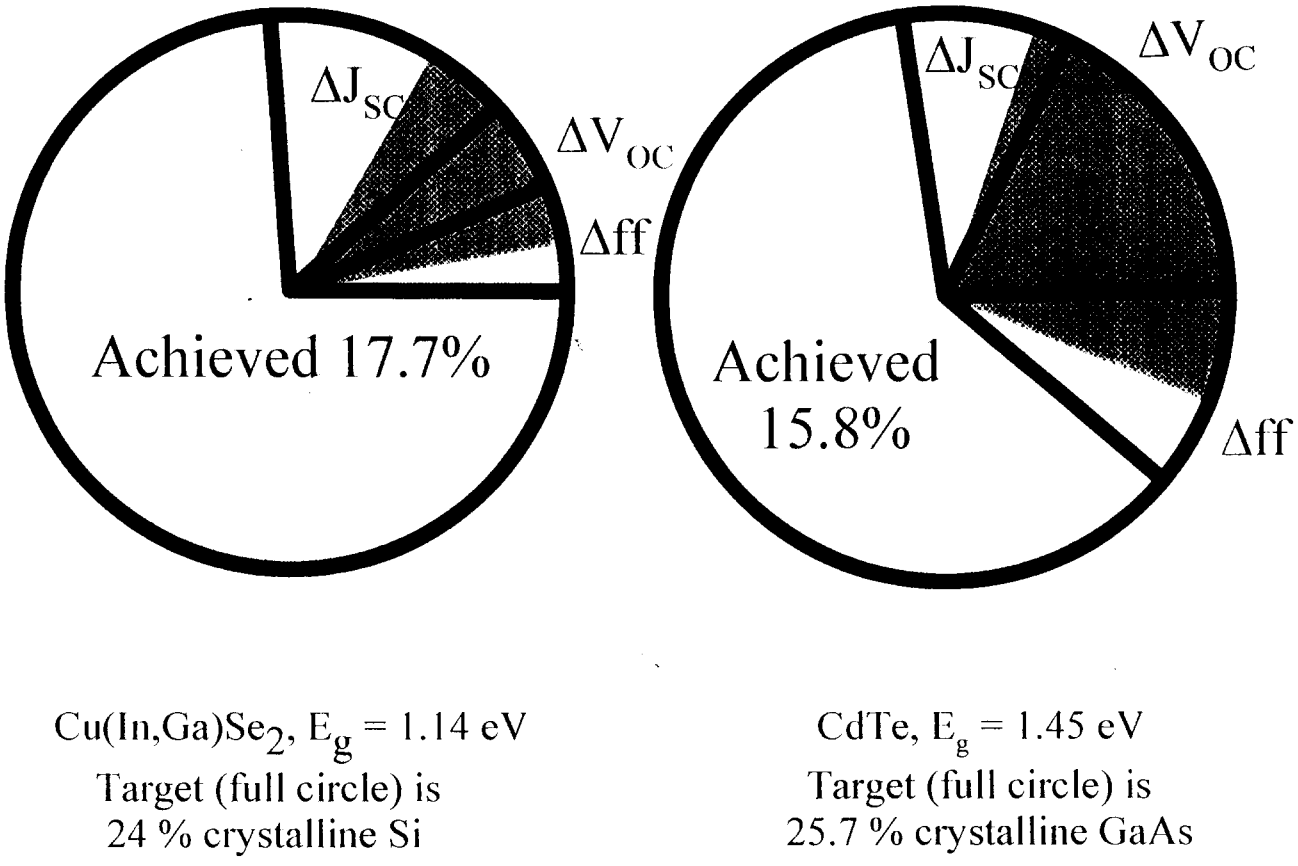


**Fig. 34.** **Comparison of highest-efficiency polycrystalline cells with crystalline counterparts. Shaded areas are due directly to granularity.**

# COMMUNICATIONS

## Publications

1. "Status of Polycrystalline Thin-Film Solar Cells," AIP Conf. Proc. **308**, 407b (1994). I.L. Eisgruber and J.R. Sites.

2. "The Large-Scale Laser Scanner: Milli-Characterization of Photovoltaic Devices and Modules, "Proc. European Photovoltaic Solar Energy Conf. **12**, 1222 (1994). R.J. Matson, K.A. Emery, I.L. Eisgruber, and L.L. Kazmerski.

3. "Six-Year Efficiency Gains for CdTe and $CuIn_{1-x}Ga_xSe_2$ Solar Cells: What Has Changed?" Proc. 1st World Photovoltaic Energy Conf, p. 119 (1994). J.R. Sites and X.X. Liu.

4. "Admittance Measurements in $Cu(In,Ga)Se_2$ Polycrystalline Thin-Film Solar Cells," Proc. 1st World Photovoltaic Energy Conf., p. 291, (1994). J.H. Scofield, M. Contreras, A.M. Gabor, R. Houfi, and J.R. Sites.

5. "Effect of Thin-Film Module Geometry on Solar Cell Current-Voltage Analysis," Proc. 1st World Photovoltaic Energy Conf., p. 271 (1994). I.L. Eisgruber, R.J. Matson, J.R. Sites, and K.A. Emery.

6. "Interpretation of Laser Scans from Thin-Film Polycrystalline Photovoltaic Modules," Proc. 1st World Photovoltaic Energy Conf., p. 283, (1994). I.L. Eisgruber, R.J. Matson, J.R. Sites, and K.A. Emery.

7. "Performance Comparison Between Polycrystalline Thin-Film and Single-Crystal Solar Cells," J.R. Sites and X.X. Liu, Prog. In Photovoltaics **3**, 307 (1995).

8. "Calculated Effect of Conduction-Band Offset on $CuInSe_2$ Solar-Cell Performance," X.X. Liu and J.R. Sites, AIP Conf. Proc. **353**, 444 (1995).

9. B.M. Keyes, J. Tuttle, J.Sites, A. Tennant, S. Asher, M. Conteras, K. Ramanathan, A. Gabor, J. Webb, R. Ahrenkiel, and R. Noufi, Proc. 11th Int. Conf. On Ternary and Multinary Materials, 1995.

10. "Analysis of CdTe Back-Contract Barriers," G. Stollwerck and J.R. Sites. Proc. 13th European PV Solar Energy Conf., P. 2020, (1995).

11. "Recent Efficiency Gains for CdTe and $CuIn_{1-x}Ga_xSe_2$ Solar Cells: What Has Changed?" J.R. Sites and X.X. Liu, Solar Energy Materials and Solar Cells, **41/42**, 373 (1996).

11. "Recent Efficiency Gains for CdTe and $CuIn_{1-x}Ga_xSe_2$ Solar Cells: What Has Changed?" J.R. Sites and X.X. Liu, Solar Energy Materials and Solar Cells, **41/42**, 373 (1996).

12. "Extraction of Individual-Cell Photocurrents and Shunt Resistances in Encapsulated Modules Using Large-Scale Laser Scanning." I.L. Eisgruber and J.R. Sites, Prog. Photovoltaics **4**, 63 (1996).

13. "$Cu(In,Ga)Se_2$ Thin Films and Solar Cells Prepared by Selenization of Metallic Precursors," B.M. Basol, V.K. Kapur, A. Halani, C.R. Leidholm, J. Sharp, J.R. Sites, A. Swartzlander, R. Matson, and H. Ullal, J. Vac. Sci Technol, **14**, 2251 (1996).

14. "Effect of CdS Thickness on CdS/CdTe Quantum Efficiency," J.E. Granata, J.R. Sites, G. Contreas-Puente, and A.D. Compaan, IEEE PVSC **25**, 853 (1996).

15. "Thin-Film Module Measurement Artifacts," I.L. Eisgruber, IEEE PVSC **25**, 829 (1996).

16. "Investigations into Alternative Substrate, Absorber, and Buffer Layer Processing for $Cu(In,Ga)Se_2$-Based Solar Cells," J.R. Tuttle, T.A. Barens, J. Keane, K.R. Ramanathan, J.E. Granata, R.N. Bhattacharya, H. Wiener, M.A. Contyraras, and R. Noufi. IEEE PVSC **25**, 797 (1996).

17. "Sodium Dependence of $Cu(In,Ga)\ Se_2$ Junction Electronics," J.E. Granata, J.R. Sites, and J.R. Tuttle, AIP Conf. Series, **394**, 621 (1996).

18. "Quantitative Incorporation of Sodium in $CuInSe_2$ and $Cu(In,Ga)Se_2$ Photovoltaic Devices," J.E. Granata, J.R. Sites, S. Asher, and R.J. Matson. IEEE PVSC **26** (1997).

19. "Advances in CIS Research at NREL," K. Ramanathan, R.N. Bhattacharya, J. Granata, J. Webb, D.Niles, M.A. Contreras, H. Wiener, F.S. Hasoon, and R. Houfi, IEEE PVSC **26** 319, (1997).

20. "$CuIn_{1-x}Ga_xSe_2$-based Photovoltaic Cells from Electrodeposited Deposited Precursor," R.N. Bhattacharya, J.E. Granata, W. Batchelor, F. Hasson, H. Wiesner, K. Ramanathan, J. Keane, R. Houfi, and J.R. Sites. SPIE Proc. **3138**, 90 (1997).

21. "Device and Materials Characterization in Manufacturing," J.R. Sites, J. Rand, L.L. Kazmerski, and J.E. Phillips, Prog. In Photovoltaics **5**, 371 (1997).

22. "Blue-Photon Modification of Nonstandard Diode Barrier in $CuInSe_2$ Solar Cells," I.L. Eisgruber, J.E. Granata, J.R. Sites, J. Hou, and J. Kessler, Solar-Energy Materials and Solar Cells. **53**, 367 (1998).

23. "Losses Due to Polycrystallinity in Thin Films," J.R. Sites, J.E. Granata, and J.F. Hiltner, Solar-Energy Materials and Solar Cells. **55**, 43 (1998).

## Graduate Degrees

1. Xiaoxiang Liu, (August 1994), Ph.D., Thesis: "Current Transport With and Without Gain-Boundary Recombination for Polycrystalline CuInSe2 Solar Cells."

2. Gunther Stollwerck, (May 1995), M.S. Thesis: "Quantitative Separation of Photon and Back-Contact Losses in CdTe Solar Cells."

3. Jon Sharp, (May 1995), M.S. Coursework/Project Degree.

4. Ingrid Eisgruber, (May 1996), Ph.D., Thesis: "Role of Nonuniformity in Thin-film Polycrystalline Module Characterization."

5. Brendon Murphy, (August 1996), M.S. Coursework/Project Degree

6. Karl Schmidt, (August 1996), M.S. Coursework/Project Degree

## Presentations

| | | | | |
|---|---|---|---|---|
| 1. | Colorado State University | Ft. Collins, CO | Sites | January 1994 |
| 2. | Institute of Energy Conversion | Newark, DE | Sites | March 1994 |
| 3. | Solarex | Newtown, PA | Sites | March 1994 |
| 4. | Energy Photovoltaics | Princeton, NJ | Sites | March 1994 |
| 5. | Siemens Solar Industries | Camarillo, CA | Sites | July 1994 |
| 6. | Solar Cells, Inc. | Toledo, OH | Sites | September 1994 |
| 7. | Oberlin College | Oberlin, OH | Sites | September 1994 |
| 8. | Dept. Of Energy Review | Denver, CO | Sites | October 1994 |
| 9. | WPVEC-1 | Kona, HI | Sites | December, 1994 |
| 10. | PVAR & D | Denver, CO | Liu | May 1995 |
| 11. | CdTe Team | Golden, CO | Granata | May 1995 |

| | | | | |
|---|---|---|---|---|
| 12. | NREL | Golden, CO | Eisgruber | August 1995 |
| 13. | Performance/Reliability Workshop | Denver, CO | Sites | September 1995 |
| 14. | European Conference | Nice, France | Stollwerck | October 1995 |
| 15. | Colorado State University | Fort Collins CO | Sites | November 1995 |
| 16. | Colorado School of Mines | Golden, CO | Sites | February 1996 |
| 17. | PVSC Tutorial | Washington, DC | Sites | May 1996 |
| 18. | PVSC Oral Paper | Washington, DC | Eisgruber | May 1996 |
| 19. | Univ. Florida Colloquium | Gainesville, FL | Sites | October 1996 |
| 20. | NREL/SNL Review | Denver, CO | Granata | November 1996 |
| 21. | CdTe Team | Newark, DE | Granata | April 1997 |
| 22. | IEC 25th Anniversary | Newark, DE | Sites | May 1997 |
| 23. | Mexican MRS | Cancun, Mexico | Sites | September 1997 |
| 24. | CdTe Team | Anaheim, CA | Sites | September 1997 |
| 25. | CIS Team | Anaheim, CA | Sites | September 1997 |
| 26. | CdTe Team | Cocoa, FL | Sites | January 1998 |